

5. SITE 1011¹

Shipboard Scientific Party²

HOLE 1011A

Date occupied: 29 April 1996
Date departed: 29 April 1996
Time on hole: 05 hr, 30 min
Position: 31°16.823'N, 117°38.018'W
Drill pipe measurement from rig floor to seafloor (m): 2032.5
Distance between rig floor and sea level (m): 10.9
Water depth (drill pipe measurement from sea level, m): 2021.6
Total depth (from rig floor, m): 2043.9
Penetration (m): 11.4
Number of cores (including cores having no recovery): 1
Total length of cored section (m): 9.5
Total core recovered (m): 9.8
Core recovery (%): 103.0
Oldest sediment cored:
Depth (mbsf): 9.50
Nature: Clayey silt
Age: Pleistocene
Comments: Missed the mudline

HOLE 1011B

Date occupied: 29 April 1996
Date departed: 1 May 1996
Time on hole: 1 day, 19 hr, 45 min
Position: 31°16.817'N, 117°38.008'W
Drill pipe measurement from rig floor to seafloor (m): 2032.5
Distance between rig floor and sea level (m): 10.9
Water depth (drill pipe measurement from sea level, m): 2021.6
Total depth (from rig floor, m): 2314.0
Penetration (m): 281.5
Number of cores (including cores having no recovery): 31
Total length of cored section (m): 281.5
Total core recovered (m): 271.1
Core recovery (%): 96.0
Oldest sediment cored:
Depth (mbsf): 272.28
Nature: Siltstone and sandstone
Age: late Miocene

Measured velocity (km/s): 1.61 at Section 28X-6, 86–89 cm
Hard rock:
Depth (mbsf): 272.28
Nature: Basalt

Basement:
Depth (mbsf): 281.50
Nature: Basalt

HOLE 1011C

Date occupied: 1 May 1996
Date departed: 2 May 1996
Time on hole: 17 hr, 45 min
Position: 31°16.819'N, 117°38.014'W
Drill pipe measurement from rig floor to seafloor (m): 2033.2
Distance between rig floor and sea level (m): 10.9
Water depth (drill pipe measurement from sea level, m): 2022.3
Total depth (from rig floor, m): 2217.5
Penetration (m): 184.3
Number of cores (including cores having no recovery): 20
Total length of cored section (m): 184.3
Total core recovered (m): 190.0
Core recovery (%): 103.0
Oldest sediment cored:
Depth (mbsf): 184.30
Nature: Clayey nannofossil chalk, nannofossil chalk
Age: late Miocene

HOLE 1011D

Date occupied: 2 May 1996
Date departed: 2 May 1996
Time on hole: 01 hr, 15 min
Position: 31°16.816'N, 117°38.019'W
Drill pipe measurement from rig floor to seafloor (m): 2031.1
Distance between rig floor and sea level (m): 10.9
Water depth (drill pipe measurement from sea level, m): 2020.2
Total depth (from rig floor, m): 2048.0
Penetration (m): 16.9
Number of cores (including cores having no recovery): 2
Total length of cored section (m): 16.9
Total core recovered (m): 17.2
Core recovery (%): 102.0

¹Lyle, M., Koizumi, I., Richter, C., et al., 1997. *Proc. ODP, Init. Repts.*, 167: College Station, TX (Ocean Drilling Program).

²Shipboard Scientific Party is given in the list preceding the Table of Contents.

Oldest sediment cored:

Depth (mbsf): 16.90
 Nature: Clayey silt, silty clay
 Age: Pleistocene

HOLE 1011E

Date occupied: 2 May 1996

Date departed: 2 May 1996

Time on hole: 08 hr, 45 min

Position: 31°16.821'N, 117°38.015'W

Drill pipe measurement from rig floor to seafloor (m): 2030.8

Distance between rig floor and sea level (m): 10.9

Water depth (drill pipe measurement from sea level, m): 2019.9

Total depth (from rig floor, m): 2173.1

Penetration (m): 142.3

Number of cores (including cores having no recovery): 16

Total length of cored section (m): 142.3

Total core recovered (m): 148.5

Core recovery (%): 104.0

Oldest sediment cored:

Depth (mbsf): 142.30
 Nature: Nannofossil silty clay
 Age: early Pliocene

Principal results: Site 1011 is the landward site of the Baja Transect, which crosses the California Current at ~30°N. Site 1011 was drilled to study both surface-water properties and water-column structure for the late Miocene to Quaternary interval. It was also drilled to sample a sedimentary section to acoustic basement to determine the nature of the basement and to gather information on the opening and subsidence of Animal Basin.

Five holes were cored with the APC/XCB at Site 1011 to a maximum depth of 281.5 mbsf, recovering an apparently continuous interval of Quaternary to upper Miocene sediments (Fig. 1). Hole 1011A is a 9.5-m-long mudline core, Hole 1011B was cored with the APC to 137.9 mbsf and extended with the XCB to 281.5 mbsf to basement. Hole 1011B was logged with the density-porosity combination tool and the combined sonic-Formation MicroScanner. Hole 1011C was cored with the APC to 136.6 mbsf and deepened with the XCB to 184.3 mbsf. Hole 1011D was cored with the APC to 16.9 mbsf. Sixteen APC cores were taken at Hole 1011E down to 142.3 mbsf. Detailed comparisons between the magnetic susceptibility and GRAPE density record generated on the MST, and high-resolution color reflectance measured with the Oregon State University system, demonstrated complete recovery of the sedimentary sequence down to 150 mbsf.

The uppermost part of the sedimentary section consists of ~25 m of siliclastic sediments with vitric ash layers and graded quartz sand beds of upper Quaternary age (Fig. 1). The underlying (180 m thick) unit is characterized by an increase in calcium carbonate and consists of silty clay and nannofossil ooze with volcanic ash layers and graded sand beds of late Miocene to Quaternary age. The section continues downward with about 60 m of late Miocene clayey diatomites and nannofossil diatomites, underlain by 14 m of poorly recovered indurated siltstone and sandstone. The oldest sedimentary is middle upper Miocene (9 Ma) and is underlain by a fine-grained vesicular basalt. Sedimentation rates throughout the section range from 15 to 40 m/m.y., averaging 30 m/m.y.

Biostratigraphic age control was provided by calcareous nannofossils and foraminifers and by siliceous diatoms and radiolarians (Fig. 1). The microfossil assemblages show evidence for strong upwelling conditions during the late Miocene and warm temperate to cool subtropical conditions with a weakening of the upwelling system in the early late Pliocene

through early Pleistocene. The late Pliocene to Quaternary assemblages indicate cooler conditions with major sea-surface temperature changes related to glacial-interglacial episodes.

Diagenetic sulfate reduction in these highly organic-rich sediments caused the dissolution of fine-grained magnetic minerals, which prevented the establishment of a magnetostratigraphy. Chemical gradients in the interstitial waters reflect organic matter diagenesis via sulfate reduction, an increase in dissolved sulfate at greater depth, the dissolution of biogenic opal, and the significant influence of authigenic mineral precipitation.

BACKGROUND AND OBJECTIVES**General Description**

Site 1011 is the landward site of the Baja Transect, which crosses the California Current at roughly 30°N. It is located about 100 km from Ensenada, Mexico, in Animal Basin, one of the outer basins in the California Borderland (Fig. 2). Water depth at Site 1011 is 2022 mbsl, but the sill depth of the basin is about 1500–1700 mbsl. The site was surveyed in detail with the *Maurice Ewing* on cruise EW9504 in 1995 (Lyle et al., 1995a, 1995b; Fig. 3). Animal Basin has relatively uniform sedimentation over moderately rugged acoustic basement, which forms occasional outcrops. At Site 1011, the sedimentary section can be divided into upper and lower sections. The upper section has relatively few reflectors that basically conform to basement topography, and thus it appears to be hemipelagic. The lower section, however, occasionally pinches and swells, and it appears to be relatively early basin fill. The acoustic signature of basement is strong in amplitude and is typical of crystalline rock.

Site Objectives

Site 1011 was drilled to study both surface water properties and water column structure for the late Miocene to Holocene interval. It was also drilled to sample a sedimentary section to acoustic basement to determine the nature of the basement and to gather information on the formation and subsidence of Animal Basin.

Deep water within Animal Basin at Site 1011 enters either through sills to the west-northwest with a minimum depth of roughly 1700 mbsl or through more local sills about 1500 m deep (Fig. 4). Benthic foraminiferal isotope data at Site 1011 should therefore be conditioned by intermediate waters between 1500 and 1700 mbsl. Not only does Site 1011 provide an inshore comparison to Site 1010, it will also be used to model changes in intermediate-water composition and will be useful in determining changes in the general water column profile since about 5 Ma.

Site 1011, the southernmost site of the coastal transect along the California Margin, preserves the record of coastal upwelling on the northern Baja California continental margin. Because the water depth at this site is relatively shallow (2022 mbsl), calcium carbonate preservation should be good, and most intervals have foraminifers for paleoceanographic study. It is the companion to Site 1010, comparing inshore conditions to those at the core of the California Current.

Site 1011 will also provide important new information about organic carbon diagenesis and about minor element geochemistry through interstitial water profiles. The only long profiles that previously existed from the California Margin are from DSDP Leg 63. During that leg only a few samples above 100 mbsf were taken, primarily because of difficulties in obtaining pristine samples with rotary cores. New interstitial water sampling at this site, especially within the upper 100 m, will better define the organic matter oxidation and the removal of oxidants from the interstitial water and sediments.

Another objective at Site 1011 was to sample the entire sedimentary column to acoustic basement (Fig. 3) so that the nature of basement can be identified and the history of basin filling can be reconstructed. Animal Basin has a small amount of sedimentary fill, so this

objective was achieved. The southern California Borderland basins have little concrete data concerning their tectonic history so drilling the sedimentary section and sampling the basement provides important new information about the evolution of the California Borderland province.

OPERATIONS

Site 1010 to Site 1011

The 82.5-nmi transit from Site 1010 to Site 1011 was accomplished in 7.5 hr at an average speed of 11.5 kt. A 3.5-kHz precision depth recorder (PDR) survey was performed while approaching Site 1011. A Datasonics 354M beacon was dropped on Global Positioning System coordinates at 1715 hr on 29 April.

Hole 1011A

Hole 1011A was spudded and a single APC Core 167-1011A-1H was taken from 0 to 9.5 mbsf (Table 1; see Table 2-CD on CD-ROM in the back pocket of this volume for a more detailed coring summary). A full barrel prevented establishing an accurate mudline, and the hole was abandoned.

Hole 1011B

The drill pipe was raised 3 m and Hole 1011B was spudded at 2245 hr on 29 April. The water depth was established at 2032.5 mbrf based on recovery of the mudline core. APC Cores 167-1011B-1H through 15H were taken from 0 to 137.9 mbsf with 103.8% recovery (Table 1). XCB Cores 167-1011B-16X through 31X were taken down to 281.5 mbsf with 89.1% recovery. Hole 1011B was terminated based on the recovery of several sections of vesicular basalt. A wiper trip was made from 281.5 mbsf up to 78 mbsf and back to the bottom of the hole where 3 m of fill was encountered. The pipe was raised to 78.5 mbsf and preparations for logging were made. Hole 1011B was logged with the density-porosity tool string from 2310 to 2113 mbrf (277.5–79.5 mbsf). The combined sonic-Formation MicroScanner tool string was run from 2310 to 2128 mbrf (277–95 mbsf). Both logging runs obtained excellent results. The pipe was pulled clear of the seafloor at 1830 hr, 1 May, ending Hole 1011B.

Hole 1011C

Hole 1011C was spudded at 1900 hr on 1 May. APC Cores 167-1011C-1H through 15H were taken from 0 to 136.6 mbsf with 103.8% recovery. XCB Cores 167-1011C-16X through 20X were taken down to 184.3 mbsf with 101.2% recovery (Table 1). Adara temperature measurements were taken on Cores 4H, 6H, 8H, 10H, and 12H (see “Physical Properties” section, this chapter). The pipe was pulled clear of the seafloor at 1215 hr on 2 May, ending Hole 1011C.

Hole 1011D

Hole 1011D was spudded at 1245 hr on 2 May. APC Cores 167-1011D-1H and 2H were taken from 0 to 16.9 mbsf with 102% recovery (Table 1). The pipe was pulled clear of the seafloor at 1330 hr on 2 May, ending Hole 1011D.

Hole 1011E

Hole 1011E was spudded at 1345 hr on 2 May. APC Cores 167-1011E-1H through 16H were taken down to 142.3 mbsf with 104.4% recovery (Table 1). The drill string was tripped back to the surface and cleared the rotary table at 0130 hr on 3 May, ending Hole 1011E.

The *JOIDES Resolution* was under way for the 7.5-hr transit to Site 1012 by 0145 hr, 3 May.

LITHOSTRATIGRAPHY

Introduction

A continuous late Miocene to Quaternary (~9.0–0.0 Ma) sedimentary sequence was recovered at Site 1011. Sediments vary from siliciclastic to interbedded mixtures of biogenic and siliciclastic components (Fig. 5). Siliciclastic clay and silt are found throughout the cored interval but are predominant in the upper portion. The lower portion consists of sediments containing variable mixtures of biogenic and/or siliciclastic components interbedded on a scale of 10 to 100 cm. Calcareous nannofossils dominate the calcareous component of the sediments, whereas a mixture of diatoms and radiolarians composes the siliceous fraction. Volcanic glass is abundant and occurs disseminated throughout the dominant lithologies and as distinct ash layers. Volcanic ash content decreases with depth, and discrete vitric ash layers are common in the upper and lower parts of the sequence.

The sediments were divided into four lithostratigraphic units based on visual core descriptions, smear-slide estimates, high-resolution GRAPE bulk density, and Formation MicroScanner data (Fig. 5). Unit I is a siliciclastic unit comprising mainly clays and silt. Unit II contains an interbedded mixture of calcareous nannofossils and siliciclastic material. Unit III predominantly consists of siliceous components interbedded and mixed with nannofossil and clay sediment. Unit IV is a siliciclastic unit containing siltstone and sandstone. Basement lithology at this site, designated Unit V, is vesicular basalt.

Description of Units

Unit I

- Hole 1011A, interval 167-1011A-1H, 1.9 (top of core)–11.4 mbsf (base of core);
 - Hole 1011B, interval 167-1011B-1H-1 through 3H-5, 0–25.4 mbsf;
 - Hole 1011C, interval 167-1011C-1H-1 through 3H-7, 0–22.3 mbsf;
 - Hole 1011D, interval 167-1011D-1H and 2H, 0–16.9 mbsf (base of core);
 - Hole 1011E, interval 167-1011E-1H-1 through 3H-7, 0–24.2 mbsf.
- Age: Quaternary, 0.0–1.0 Ma.

Unit I is predominantly composed of dark gray (5Y 4/1 to 5Y 5/1) to gray (10Y 6/1) siliciclastic clay and silt with scattered dark gray to black (N2 to N4) vitric ashes and graded sand layers. Clay content varies from 20% to 70% based on smear-slide observations. The silt component consists mainly of feldspar (0% to 15%), quartz (0% to 28%), fresh and altered volcanic glass fragments (0% to 15%), and varying but minor components of biotite and amphibole.

Unit II

- Hole 1011B, interval 167-1011B-3H-6 through 22X-7, 25.4–204.3 mbsf;
 - Hole 1011C, interval 167-1011C-4H-1 through 20X-7, 22.3–184.3 mbsf (base of core);
 - Hole 1011E, interval 167-1011E-4H-1 through 16H, 24.2–142.3 mbsf (base of core).
- Age: Quaternary to late Miocene, 1.0–7.5 Ma.

The transition from Unit I to Unit II is marked by the first occurrence of abundant biogenic components as noted by a change in sediment color to olive gray (10Y 6/2) and light olive gray (5Y 6/2). Unit II consists of moderately bioturbated, gradationally interbedded lithologies with varied mixtures of calcareous nannofossil and siliciclastic components. Unit II is divided into three subunits based on the relative abundance of the major components. Contacts between subunits are not strictly defined because of the gradational nature of in-

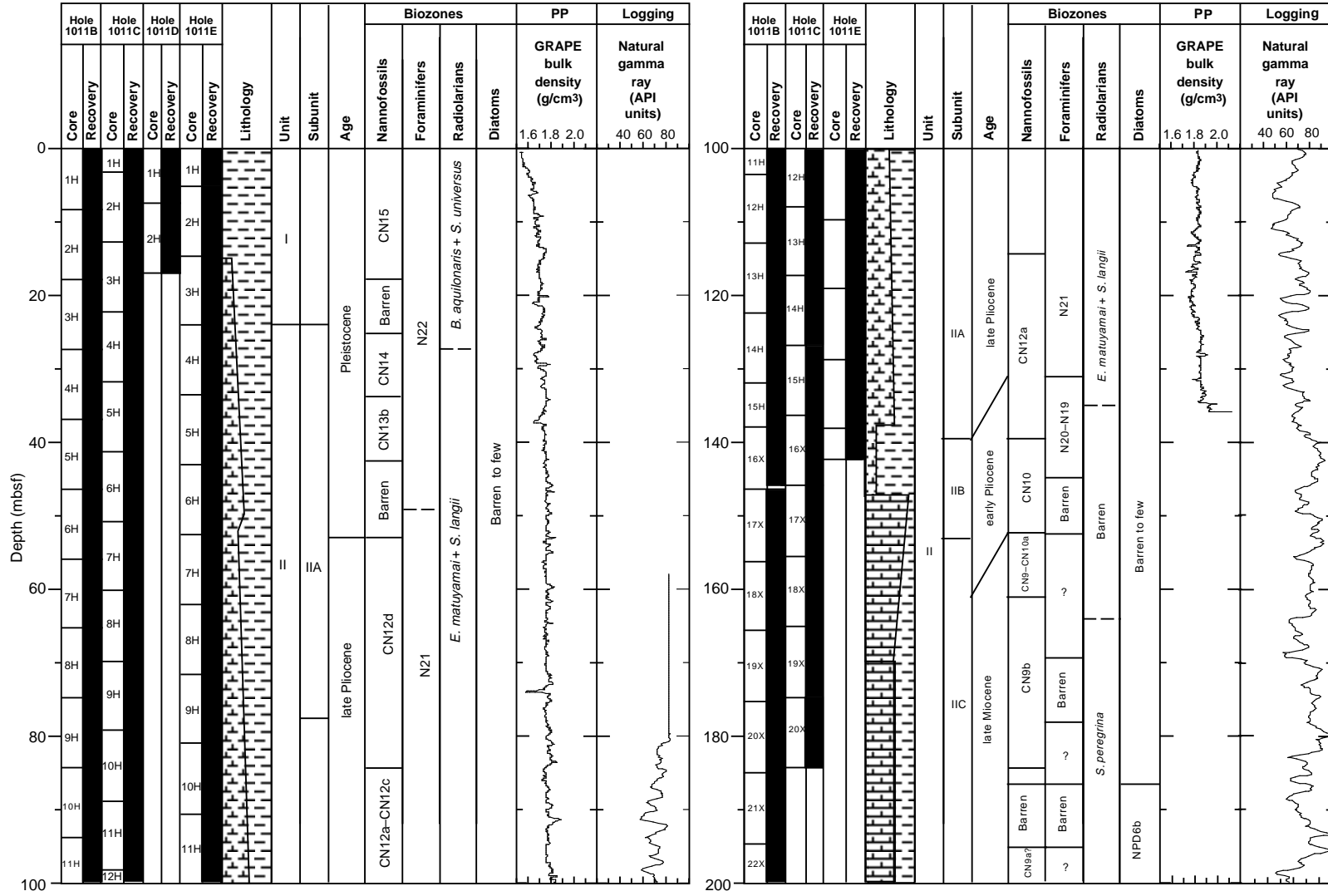


Figure 1. Site 1011 master column.

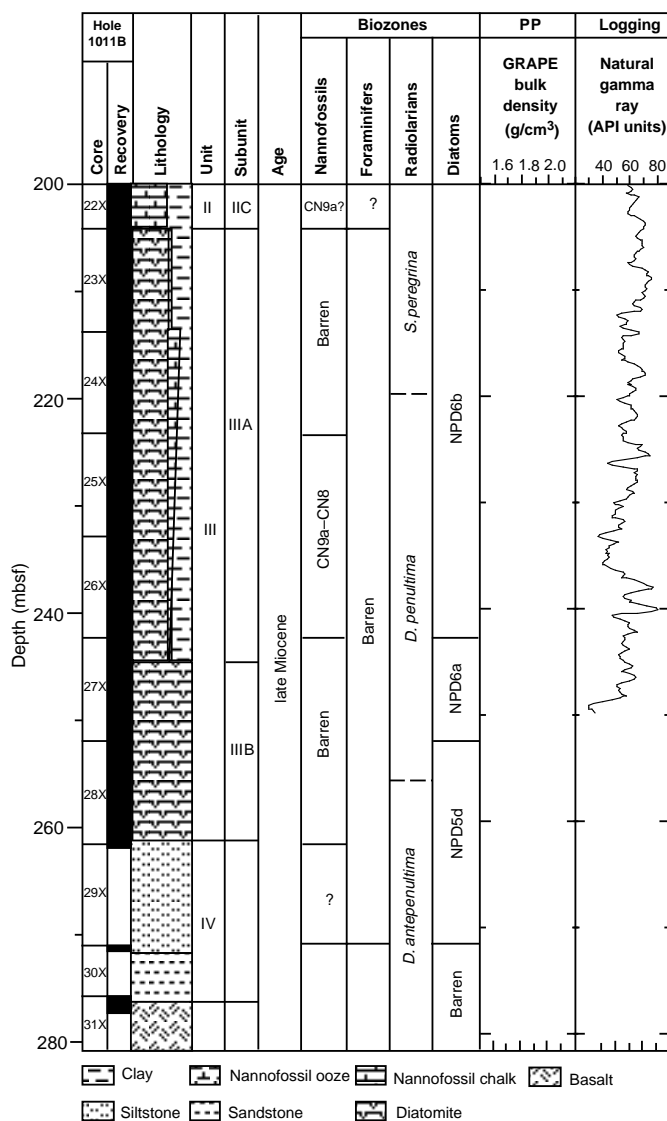


Figure 1 (continued).

terbedding in this unit; thus, “intervals” given below are only approximate.

Subunit IIA

Hole 1011B, interval 167-1011B-3H-6 through 14H-7, 25.4–131.9 mbsf;
Hole 1011C, interval 167-1011C-4H-1 through 14H-7, 22.3–126.8 mbsf;
Hole 1011E, interval 167-1011E-4H-1 through 16H, 24.2–142.3 mbsf
(base of core).

Subunit IIA consists of interbedded olive gray (5Y 4/2 to 10Y 4/1) silty clay and light olive gray (5Y 6/2) nannofossil ooze on the decimeter to meter scale. The percentage of CaCO₃ increases down-core through this subunit inversely to silt content (see “Inorganic Geochemistry” section, this chapter). Thin graded beds composed of quartz feldspar sand occur throughout the subunit down to 97.0 mbsf. Vitric ash layers occur down to 118 mbsf.

Subunit IIB

Hole 1011B, interval 167-1011B-15H-1 through 16X-7, 131.9–146.5 mbsf;
Hole 1011C, interval 167-1011C-15H-1 through 16X-7, 126.8–145.8 mbsf.

The upper contact of Subunit IIB with the Subunit IIA is gradational, marked by a decrease in calcareous nannofossils and an in-

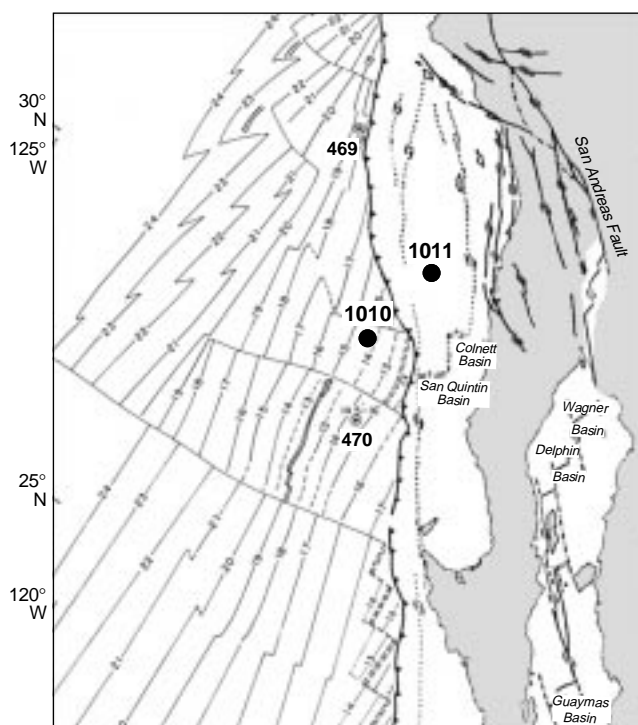


Figure 2. Location map for Site 1011. Crustal ages from Lonsdale (1991). Site 1011 is located about 100 km west of Ensenada, Mexico, in a basin of late to middle Miocene age. Locations of ODP Site 1010 and DSDP Sites 469 and 470 are shown for reference.

crease in the silty clay component. This subunit corresponds to decreased porosity and void ratios (see “Physical Properties” section, this chapter). The lithology consists of gradationally interbedded grayish olive to olive gray (10Y 4/2 to 5Y 4/2) silty clay and light gray to pale olive (5Y 7/2) silty clay with nannofossils. The overall percentage of CaCO₃ is low in this interval (see “Inorganic Geochemistry” section, this chapter).

Subunit IIC

Hole 1011B, interval 167-1011B-17X-1 through 22X-7, 146.5–204.3 mbsf;
Hole 1011C, interval 167-1011C-16X-7 through 20X-7, 145.8–184.3 mbsf (base of core).

The contact of Subunit IIC with Subunit IIB is gradational and defined by increased lithification but is otherwise compositionally similar to Subunit IIA. The boundary is coincident with the corresponding change from APC to XCB coring. This subunit consists of gradationally interbedded pale olive (10Y 4/2 to 5Y 4/2) nannofossil chalk and olive gray to dark olive gray (5Y 4/2 to 5Y 3/2) nannofossil claystone on an ~1-m scale (Fig. 6). Ash and volcanic sand layers occur below 184.0 mbsf.

Unit III

Hole 1011B, interval 167-1011B-23X-1 through 28X-7, 204.3–262.1 mbsf.
Age: late Miocene, 8.5–7.5 Ma.

The contact between Unit II and Unit III is marked by a change in the biogenic component from calcareous nannofossils to siliceous diatoms and radiolarians and a change in color to dark olive gray (10Y 5/2) diatomite with silty clay and dark grayish brown (2.5Y 4/2) diatomite with nannofossils. Based on smear-slide observations, dia-

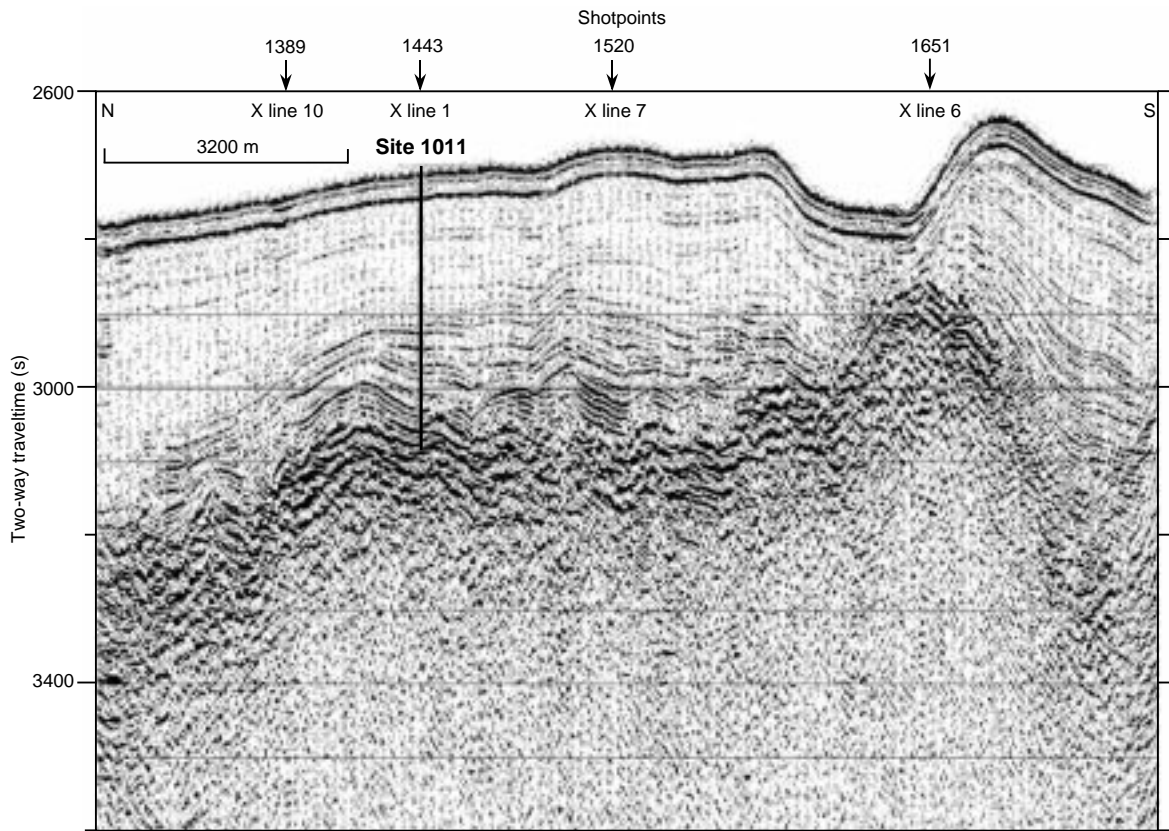


Figure 3. Seismic reflection profile through Site 1011 (Line EW9504 CAM2-2; Lyle et al., 1995b). Two prominent seismic units can be identified in the sediment column: an upper transparent unit and a lower, more reflective one. On y-axis, (s) = milliseconds.

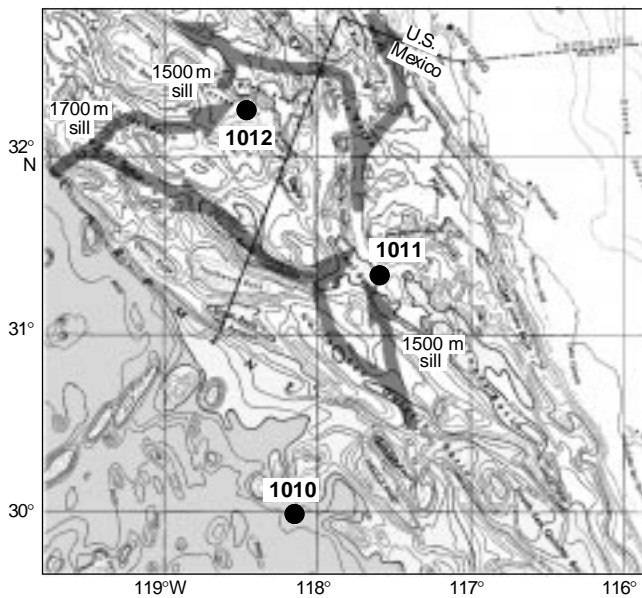


Figure 4. Flow paths for deep water into the Animal Basin. A deep sill of 1700 mbsl exists about 150 km to the west-northwest of the basin, while local sills are at depths of about 1500 mbsl.

toms compose 50% to 70% of the sediment and nannofossils make up between 0% and 15%. GRAPE bulk density decreases at this transition (see “Physical Properties” section, this chapter) and there is a drop in the %CaCO₃ (see “Inorganic Geochemistry” section, this chapter). Formation MicroScanner data also show a distinct change between Units II and III (see “Downhole Measurements” section, this chapter). Unit III is divided into two subunits; the upper part is composed of less pure diatomite than the lower. GRAPE bulk density values also change at this boundary.

Subunit IIIA

Hole 1011B, interval 167-1011B-23X-1 through 27X-2, 204.3–245.8 mbsf.

Subunit IIIA is composed of diatomite that contains between 60% and 70% diatoms and from 0% to 15% of both nannofossils and clay. The sediments are gradationally interbedded on a 10–30 cm scale. Sediments are well-bioturbated and contain abundant *Zoophycos* and *Chondrites* trace fossils (Fig. 7). Vitric ashes occur intermittently throughout this subunit.

Subunit IIIB

Hole 1011B, interval 167-1011B-27X-3 through 28X-7, 245.8–262.1 mbsf.

Subunit IIIB consists of dark grayish brown (2.5Y 3/2) diatomite (composed of approximately 75% diatoms based on smear-slide observations) interbedded with minor grayish brown (2.5Y 5/2) diatomite with clay and silty clay layers.

Table 1. Coring summary for Site 1011.

Core	Date (1996)	Time	Top (mbsf)	Bottom (mbsf)	Length cored (m)	Length recovered (m)	Recovery (%)
167-1011A-1H	April 30	0520	1.9	11.4	9.5	9.84	103.0
167-1011B-1H	April 30	0600	0.0	8.4	8.4	8.40	100.0
2H	April 30	0645	8.4	17.9	9.5	9.83	103.0
3H	April 30	0730	17.9	27.4	9.5	9.94	104.0
4H	April 30	0810	27.4	36.9	9.5	9.85	103.0
5H	April 30	0850	36.9	46.4	9.5	9.90	104.0
6H	April 30	0930	46.4	55.9	9.5	10.03	105.6
7H	April 30	1010	55.9	65.4	9.5	9.87	104.0
8H	April 30	1045	65.4	74.9	9.5	9.82	103.0
9H	April 30	1120	74.9	84.4	9.5	10.04	105.7
10H	April 30	1220	84.4	93.9	9.5	9.98	105.0
11H	April 30	1255	93.9	103.4	9.5	9.76	103.0
12H	April 30	1335	103.4	112.9	9.5	9.72	102.0
13H	April 30	1420	112.9	122.4	9.5	9.78	103.0
14H	April 30	1515	122.4	131.9	9.5	9.96	105.0
15H	April 30	1600	131.9	137.9	6.0	6.26	104.0
16X	April 30	1755	137.9	146.5	8.6	8.09	94.0
17X	April 30	1920	146.5	156.2	9.7	9.85	101.0
18X	April 30	2035	156.2	165.7	9.5	9.95	105.0
19X	April 30	2135	165.7	175.4	9.7	9.65	99.5
20X	April 30	2235	175.4	185.0	9.6	9.58	99.8
21X	April 30	2330	185.0	194.6	9.6	9.82	102.0
22X	May 1	0035	194.6	204.3	9.7	9.76	100.0
23X	May 1	0135	204.3	213.9	9.6	9.60	100.0
24X	May 1	0230	213.9	223.5	9.6	9.66	100.0
25X	May 1	0330	223.5	233.2	9.7	9.91	102.0
26X	May 1	0415	233.2	242.8	9.6	9.87	103.0
27X	May 1	0510	242.8	252.4	9.6	9.89	103.0
28X	May 1	0630	252.4	262.1	9.7	9.69	99.9
29X	May 1	0730	262.1	271.7	9.6	0.36	3.8
30X	May 1	0910	271.7	276.4	4.7	0.62	13.2
31X	May 1	1115	276.4	281.5	5.1	1.61	31.5
167-1011C-1H	May 2	0215	0.0	3.3	3.3	3.34	101.0
2H	May 2	0245	3.3	12.8	9.5	10.11	106.4
3H	May 2	0325	12.8	22.3	9.5	9.53	100.0
4H	May 2	0430	22.3	31.8	9.5	10.15	106.8
5H	May 2	0500	31.8	41.3	9.5	9.88	104.0
6H	May 2	0550	41.3	50.8	9.5	10.06	105.9
7H	May 2	0615	50.8	60.3	9.5	9.90	104.0
8H	May 2	0700	60.3	69.8	9.5	10.03	105.6
9H	May 2	0745	69.8	79.3	9.5	9.97	105.0
10H	May 2	0845	79.3	88.8	9.5	10.01	105.3
11H	May 2	0915	88.8	98.3	9.5	9.45	99.5
12H	May 2	1025	98.3	107.8	9.5	9.99	105.0
13H	May 2	1110	107.8	117.3	9.5	9.82	103.0
14H	May 2	1145	117.3	126.8	9.5	9.35	98.4
15H	May 2	1240	126.8	136.3	9.5	9.92	104.0
16X	May 2	1430	136.3	145.8	9.5	9.63	101.0
17X	May 2	1530	145.8	155.5	9.7	9.70	100.0
18X	May 2	1630	155.5	165.0	9.5	9.69	102.0
19X	May 2	1720	165.0	174.7	9.7	9.67	99.7
20X	May 2	1820	174.7	184.3	9.6	9.77	102.0
167-1011D-1H	May 2	2000	0.0	7.4	7.4	7.38	99.7
2H	May 2	2030	7.4	16.9	9.5	9.86	104.0
167-1011E-1H	May 2	2100	0.0	5.2	5.2	5.17	99.4
2H	May 2	2130	5.2	14.7	9.5	9.63	101.0
3H	May 2	2200	14.7	24.2	9.5	10.00	105.2
4H	May 2	2230	24.2	33.7	9.5	9.85	103.0
5H	May 2	2300	33.7	43.2	9.5	9.84	103.0
6H	May 2	2330	43.2	52.7	9.5	9.98	105.0
7H	May 3	0000	52.7	62.2	9.5	10.07	106.0
8H	May 3	0030	62.2	71.7	9.5	9.72	102.0
9H	May 3	0100	71.7	81.2	9.5	10.07	106.0
10H	May 3	0130	81.2	90.7	9.5	9.90	104.0
11H	May 3	0145	90.7	100.2	9.5	10.11	106.4
12H	May 3	0225	100.2	109.7	9.5	9.90	104.0
13H	May 3	0250	109.7	119.2	9.5	10.05	105.8
14H	May 3	0315	119.2	128.7	9.5	10.06	105.9
15H	May 3	0345	128.7	138.2	9.5	10.06	105.9
16H	May 3	0415	138.2	142.3	4.1	4.11	100.0

Note: Table 2, on the CD-ROM, back pocket, this volume, is a more detailed coring summary.

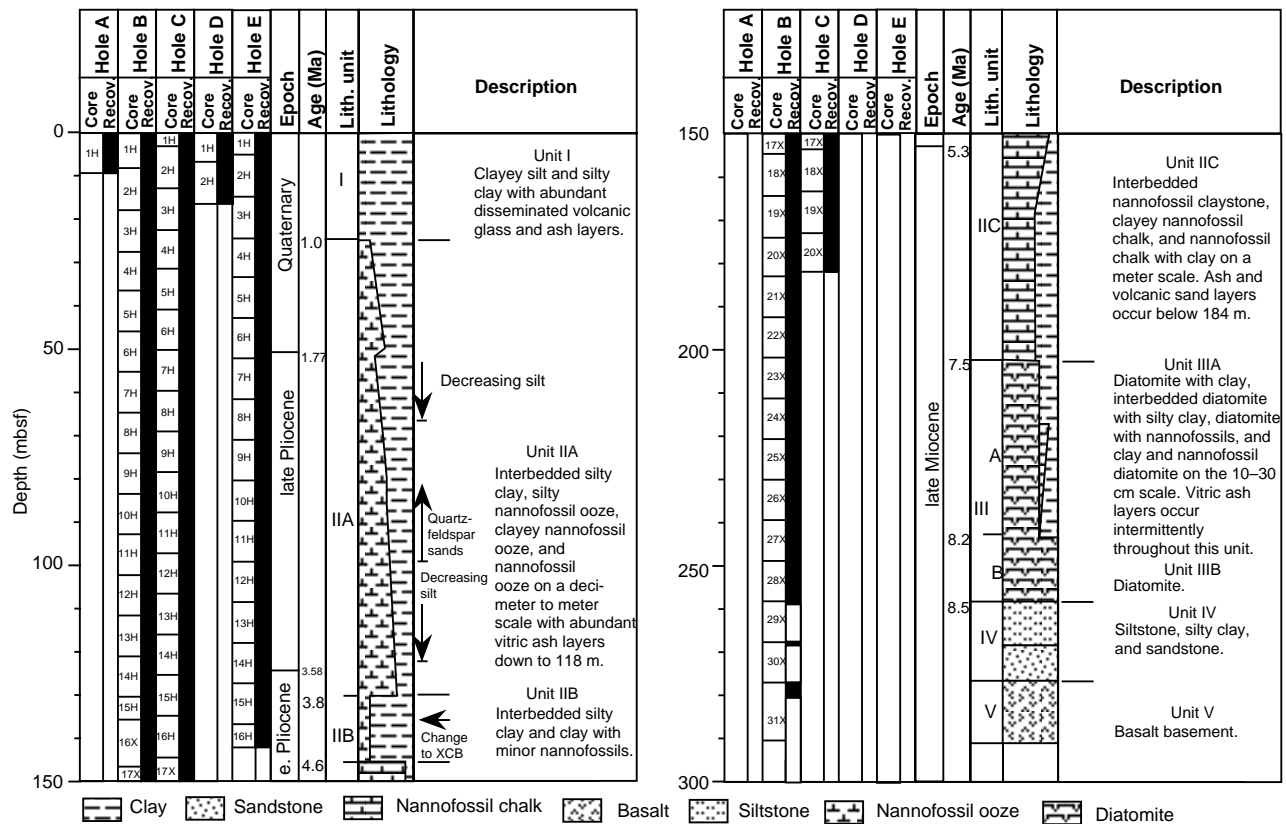


Figure 5. Site 1011 lithostratigraphic summary (0–278.3 mbsf).

Unit IV

Hole 1011B, interval 167-1011B-29X and 30X, 262.1–276.4 mbsf.
Age: late Miocene, ~9.0–8.5 Ma.

The contact between Unit III and Unit IV is marked by a change from biogenic to indurated siliciclastic lithologies. The upper part of the unit is composed of black (5Y 2.5/1) silicified siltstone interbedded with olive gray (5Y 4/2) silty clay. The lower part of Unit IV is composed of silicified siltstone and coarse-grained quartz feldspar sandstone. Recovery of Unit IV was quite poor (13% to 31%), and the recovered rock was highly fractured.

Unit V

Hole 1011B, interval 167-1011B-31X, 276.4–281.5 mbsf.

Basement was reached at 276.4 mbsf, and 1.89 m of finely crystalline, vesicular basalt was recovered.

Depositional History

Sediments at Site 1011 consist of interbedded siliciclastic clays, nannofossil ooze, and siliceous ooze. Volcanic ashes occur every 10–15 m in the upper part of the sedimentary sequence, are absent between 118 and 184 mbsf, and occur intermittently in the lower part. Siliceous sediments dominate the older portion of the sequence from about 8.5 to 7.5 Ma. This interval is characterized by decimeter-scale interbedding of siliceous ooze dominated by diatoms with clay and minor nannofossil ooze, similar to shoreward basin deposits of the

Monterey Formation of California during this time (Ingle, 1981). Siliceous ooze deposition ceased in the late Miocene (7.5 Ma) and was followed by an interval of interbedded nannofossil ooze and clay from about 7.5 to 1.0 Ma. A marked decrease in nannofossil content and increase in silt and clay content occurred between 4.6 and 3.8 Ma, accompanied by a decrease in sedimentation rate (~1.7 cm/k.y.; see “Biostratigraphy” section, this chapter). This was followed by a return to more rapid sedimentation rates (~4 cm/k.y.; see “Biostratigraphy” section, this chapter) and interbedded nannofossil ooze and silty clay until ~1.0 Ma (Quaternary) when sedimentation changed to siliciclastic clays and silt. The deposition of graded sand beds began at about 3.2–3.1 Ma, which may reflect tectonism associated with the onset of the tectonic uplift documented in the Santa Maria Basin area of the central California Margin at this time (McCroery et al., 1995).

BIOSTRATIGRAPHY

The sedimentary sequence recovered from the five holes cored at Site 1011 consists of an apparently continuous 281.5-m-thick interval of upper Miocene to Quaternary sediments. The section includes an upper 132-m-thick sequence containing abundant planktonic foraminifers and calcareous nannofossils, few benthic foraminifers, and rare to absent diatoms and radiolarians from the late early Pliocene to the Quaternary. This is underlain by a 48-m-thick sequence of late late Miocene to early Pliocene age characterized by rare and sporadic assemblages of planktonic foraminifers, few to abundant calcareous nannofossils, and generally uncommon diatoms and radiolarians. Below this interval, a 110-m-thick sequence of rapidly deposited diatom-rich sediments of late Miocene age was recovered. These sedi-

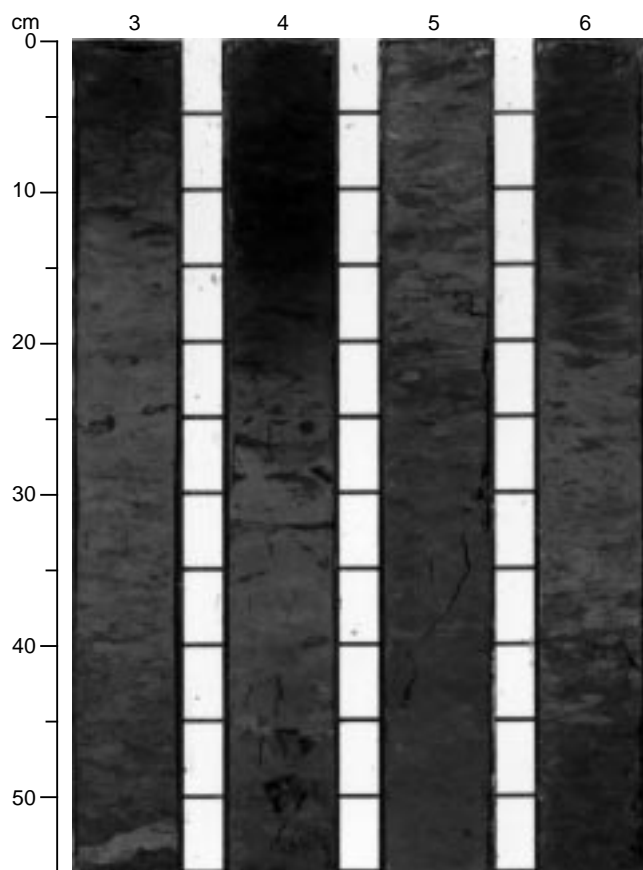


Figure 6. Cyclic interbedding of nanofossil chalk and nanofossil claystone with gradational, burrowed transitions (Samples 167-1011C-19X-3, 0–55 cm, 19X-4, 0–55 cm, 19X-5, 0–55 cm, and 19X-6, 0–55 cm).

ments contain abundant diatoms and radiolarians. Calcareous nanofossils and planktonic foraminifers are rare or absent. Benthic foraminifers assemblages are less consistently present. The base of the sedimentary sequence is assigned to the middle late Miocene diatom *Denticulopsis dimorpha* Zone, indicating an age of approximately 9 Ma (last occurrence of *D. dimorpha* between 252 and 262 mbsf).

A well-constrained biostratigraphy and chronology for Hole 1011B is provided by the combination of all microfossil groups (Tables 3–9). Assigned ages based on foraminifers, calcareous nanofossils, diatoms, and radiolarians are similar between Holes 1011B and 1011C. An age/depth plot at Hole 1011B (Fig. 8) shows an almost continuous sedimentation rate in the sequence, with no hiatuses.

Dominant cold species of planktonic foraminifers, diatom, and radiolarian assemblages exhibit evidence of strong upwelling conditions during the late Miocene. The predominance of temperate foraminiferal species in early late Pliocene through early Pleistocene assemblages, and rare occurrences of diatoms and radiolarians, indicate warm temperate to cool subtropical conditions with a weakening of the upwelling system. Late Pliocene to Quaternary planktonic foraminiferal assemblages indicate cooler conditions with major sea-surface temperature changes related to glacial-interglacial episodes. Fewer occurrences of subtropical forms suggest generally cooler conditions than during the early and early late Pliocene.

The sequence at Site 1011 offers good opportunities for paleoceanographic investigations on the weakening of the late Miocene

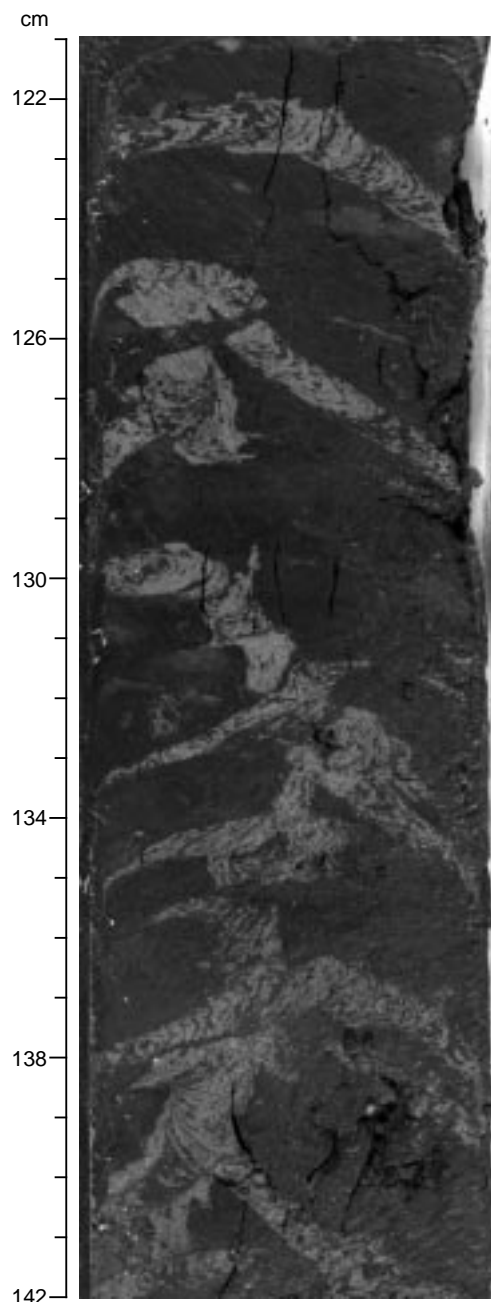


Figure 7. Splendid *Zoophycos* trace fossil in diatomite with clay (Sample 167-1011B-26X-5, 121–142 cm).

extensive upwelling of cool waters and the establishment of Pleistocene glacial/interglacial variations of the California Current.

Planktonic Foraminifers

Site 1011 contains an excellent planktonic foraminiferal sequence down to 132 mbsf of Quaternary to late early Pliocene age (Tables 3, 4). Below this, assemblages are sporadic and poor. Planktonic foraminifers are highly abundant to common throughout most of the Quaternary and Pliocene (0 to 132 mbsf; Samples 167-1011B-1H-CC to 14H-CC), below which they are rare or absent. Preservation in gen-

Table 3. Ranges of planktonic foraminifers in Hole 1010B.

Core, section, interval	Depth (mbsf)	Abundance	Preservation	<i>Globorotalia truncatulinoides</i>	<i>Neoglobobquadrina duterrei</i>	<i>Globorotalia tosaensis</i>	<i>Neoglobobquadrina humerosa</i>	<i>Globorotalia iriflata</i>	<i>Globorotalia puncticulata</i>	<i>Globorotalia crassaformis</i>	<i>Neoglobobquadrina asanoi</i>	<i>Neoglobobquadrina</i> sp. "rounded"	<i>Sphaeroidinella delhiscens</i>	<i>Neoglobobquadrina pachyderma</i> dex.	<i>Neoglobobquadrina pachyderma</i> sin.	<i>Globigerina bulloides</i>	<i>Orbulina universa</i>	<i>Globigerinoides conglobatus</i>	<i>Globigerinoides ruber</i>	<i>Globorotalia tumida</i>	<i>Globorotaloides hexagona</i>	<i>Sphaerodinelles psis seminulina</i>	<i>Globigerina woodi</i>	<i>Globorotalia scitula</i>	<i>Globorotalia hirsuta</i>	<i>Globigerinita glutinata</i>	<i>Globigerinoides trilobus</i>	<i>Hastigerina aequilateralis</i>	<i>Globigerina quinqueloba</i>	<i>Globigerina umbilicata</i>	<i>Globorotalia crassula</i>	<i>Globigerina apertura</i>	<i>Globigerinoides sacculifer</i>	<i>Globigerinoides obliquus</i>						
167-1010B-1H-CC	11.9	A	G	R	A			R		C				A	F	A			C		R			R	R															
2H-CC	17.9	A	G											A	A	A			R					R	R															
3H-CC	27.4	A	G											A	C	A			R		R			R	R															
4H-CC	36.9	A	G				R	R		R				A	A	A			R					R	R															
5H-CC	46.4	C	M											A	A	R	R		R				R	R																
6H-CC	55.9	R	M				R							R	R	R																								
7H-CC	64.9	A	G				C							A	A	R																								
8H-CC	74.9	A	M				R	R		R	A			A	R	R								R																
9H-CC	84.4	C	M					R			A			R	A	R																								
10H-CC	93.9	A	G				R		C	R	A	A	A	A	R	A	R						R																	
11H-CC	103.0	C	M				A		R		A			R	R	R			R	C				R																
12H-CC	112.9	F	M					A	R						R	R			R	R		R																		
13H-CC	122.4	C	M				A	A	R		A	C			R	R			R	R																				
14H-CC	132.0	F/R	M/P				A		R		A	R			R	R			R	R																				
15H-CC	138.0	R	P								R				R	R			R	R																				
16X-CC	146.5	B																																						
17X-CC	156.2	R	P													R																								
18X-CC	165.7	R	P													C																								
19X-CC	175.4	B																																						
20X-CC	185.0	R	P													R																								
21X-CC	194.0	B																																						
22X-CC	204.3	R	M													R																								
23X-CC	213.9	B																																						
24X-CC	223.5	B																																						
25X-CC	233.2	B																																						
26X-CC	243.0	B																																						
27X-CC	253.0	B																																						
28X-CC	262.0	B																																						
29X-CC	272.0	B																																						

Note: See "Explanatory Notes" chapter for abbreviations.

Table 4. Ranges of planktonic foraminifers in Hole 1011C.

Core, section, interval	Depth (mbsf)	Abundance	Preservation	<i>Globorotalia truncatulinoides</i>	<i>Neogloboquadrina dutertrei</i>	<i>Globorotalia tosaensis</i>	<i>Neogloboquadrina humerosa</i>	<i>Globorotalia inflata</i>	<i>Globorotalia puncticulata</i>	<i>Globorotalia crassaformis</i>	<i>Neogloboquadrina asanoi</i>	<i>Neogloboquadrina</i> sp. "rounded"	<i>Sphaerodinelletta dehiscentes</i>	<i>Neogloboquadrina pachyderma</i> dex.	<i>Neogloboquadrina pachyderma</i> sin.	<i>Globigerina bulloides</i>	<i>Globigerinoides conglobatus</i>	<i>Globigerinoides ruber</i>	<i>Globorotalia tumida</i>	<i>Sphaerodinelletta seminulina</i>	<i>Globigerinoides trilobus</i>	<i>Globigerina umbilicata</i>	<i>Globorotalia crassula</i>	<i>Globigerinoides sacculifer</i>	<i>Globigerinoides obliquus</i>
167-1011C-1H-CC	3.3	A	G					C						R	A	A									
2H-CC	12.8	A	G					R						R	A	A									
3H-CC	22.3	A	M					C						A		C									
4H-CC	31.8	A	G	A			C	A						A		A									
5H-CC	41.3	A	G	C			R	C						C	C	C									
6H-CC	50.8	A	G	F		F	C	C	F					C		A									R
7H-CC	60.3	A	G				C	C						A		A									
8H-CC	69.8	A	G				A	C			A			A	A	A									
9H-CC	79.3	A	M				A	C			A			A	A	A									
10H-CC	88.8	A	G				C	R	F		A	A		F	A	A									
11H-CC	98.3	F	P				R				R	A		A		R									
12H-CC	107.8	A	G				A	F			R	A		A		A									
13H-CC	117.3	A	G				A				C	A		A		A									
14H-CC	126.8	A	G				A				A	A		R		A									
15H-CC	136.3	F	P				A				A	A		A		A									
16X-CC	145.8	F	P													C		R							R

Note: See "Explanatory Notes" chapter for abbreviations.

eral becomes worse with increasing depth in the sequence. Assemblages are well preserved from the top of the sequence to 37 mbsf, are moderately well preserved from 37 mbsf to 122 mbsf, are consistently poorly preserved from 122 mbsf to 166 mbsf, and are often absent or poorly preserved below this interval. Specimen fragmentation is pervasive, and robust forms often dominate. The sequence at Site 1011 exhibits a series range change in a number of planktonic foraminifers from the late early Pliocene to the latest Quaternary.

Hole 1011B

An uppermost zone of Quaternary age is indicated by the co-occurrence of *Globorotalia truncatulinoides* and *Neogloboquadrina dutertrei* (from top of sequence to Sample 167-1011B-2H-CC). This zone correlates with Zone N22–N23 of tropical regions, based on the FO of *G. truncatulinoides*. This zone is underlain by a zone marked by the absence of *G. truncatulinoides* and *N. dutertrei*, and the sporadic concurrence of *Globorotalia tosaensis*, *Neogloboquadrina humerosa*, *Globorotalia inflata*, and *Globorotalia crassaformis*. This zone ranges from Samples 167-1011B-3H-CC to 7H-CC. *G. tosaensis* was observed as a single specimen in 4H-CC. The presence of *G. tosaensis* normally defines Zone N21 of upper Pliocene age, but at higher latitudes in the northeastern Pacific, *G. tosaensis* was observed within the lower Quaternary (Zellers, 1995). The base of this zone is marked by the LO of *Neogloboquadrina asanoi*.

The top of the underlying zone is marked by them LO of *N. asanoi*, which occurs immediately above the LO of *Globorotalia puncticulata*. This zone extends from Samples 167-1011B-8H-CC to 13H-CC. The base of the zone is marked by the FO of *Globorotalia inflata* and *Globorotalia puncticulata*. This zone is of late Pliocene age and is correlated with the lower part of Zone N21. Much of the zone is marked by the concurrent range of *N. asanoi* and *G. puncticulata*, as well as the presence of sporadic *G. inflata* and *N. humerosa*.

The top of the underlying zone is marked by the FO of *G. inflata* and *Globorotalia crassaformis*. This zone is defined by the presence of *G. crassaformis* and absence of *G. inflata* and *G. puncticulata*. The

base of this zone could not be defined because planktonic foraminiferal assemblages in this interval were too rare.

Planktonic foraminiferal assemblages below Sample 167-1011B-15H-CC are insufficiently abundant or absent to allow biostratigraphic subdivision. Sparse assemblages, when present, are dominated by *Globigerina bulloides*. No marker species were found.

Hole 1011C

The biostratigraphic sequence of planktonic foraminifers in Hole 1011C is similar to that of Hole 1011B with one important exception. In Hole 1011B, *G. truncatulinoides* was seen only in the uppermost part of the sequence from 18 mbsf to the top (Samples 167-1011B-1H-CC and 2H-CC). In Hole 1011C the FO of *G. truncatulinoides* was observed much lower in the sequence at 50.8 mbsf (Sample 167-1011C-6H-CC). At its first appearance in Hole 1011C, *G. truncatulinoides* is a primitive form grading into *G. tosaensis*. Specimens of *G. truncatulinoides* exhibit a weak peripheral keel and the keel is absent on the final chamber. Thus, Hole 1011C has preserved the initial evolutionary appearance of *G. truncatulinoides* with an assigned age of 1.77 Ma.

The upper Neogene planktonic foraminiferal assemblages in Site 1011 define three intervals that are associated with paleoceanographic-paleoclimatic change. Late Miocene assemblages from Sample 167-1011B-22X-CC to 15H-CC are associated with rich radiolarian and diatom assemblages indicative of major upwelling conditions. The planktonic foraminiferal assemblages are almost exclusively represented by *G. bulloides*, a well-known upwelling species. Few other taxa are present.

The early through lower upper Pliocene assemblages are relatively diverse and are dominated by temperate forms, in addition to rare occurrences of forms with subtropical affinity such as *Globorotalia tumida*, *Globigerinoides sacculifer*, *Globigerinoides obliquus*, and *Sphaerodinelletta seminulina*. These assemblages generally lack *Neogloboquadrina pachyderma* (dextral), a cool-temperate form in this region. This assemblage indicates dominance of warm temperate

Table 5. Abundance of calcareous nannofossils at Site 1011.

Zone	Core, section, interval (cm)	Depth (mbsf)	Preservation	Abundance	<i>Emiliana huxleyi</i>	<i>Pseudoemiliana lacunosa</i>	<i>Helicosphaera carteri</i>	<i>Helicosphaera sellii</i>	<i>Gephyrocapsa oceanica</i> s.l.	<i>Gephyrocapsa</i> sp. 3	<i>Gephyrocapsa</i> small	<i>Gephyrocapsa</i> large	<i>Discoaster brauneri</i>	<i>Discoaster triradiatus</i>	<i>Discoaster pentaradiatus</i>	<i>Discoaster surculus</i>	<i>Discoaster tamalis</i>	<i>Discoaster asymmetricus</i>	<i>Sphenolithus</i> spp.	<i>Reticulofenestra pseudoubilicus</i>	<i>Ceratholithus</i> spp.	<i>Ceratholithus telesmus</i>	<i>Ceratholithus acutus</i>	<i>Ceratholithus rugosus</i>	<i>Amaurolithus amplifolius</i>	<i>Amaurolithus</i> spp.	<i>Discoaster berggrenii/quinqueramus</i>	<i>Minylitha conwallis</i>	<i>Coccolithus pelagicus</i>	<i>Calcidiscus macinirei</i> >11 µm	<i>Calcidiscus leptoporus</i>		
CN15-CN14b	167-1011A-1H-CC	11.4	M/G	C			C			P	F	C										R										R	
CN15	167-1011B-1H-CC	8.4	M	C	A		C		F	R	A																			F	R		
CN15	2H-CC	12.9	G	A	A						C																						
CN14	3H-CC	27.4	G	B																													
CN14	4H-CC	36.9	G	A								A																					
CN13b	5H-CC	46.4	G	A			C		C	R		R									F	R							C		R		
CN13b	6H-CC	55.9	G	B																													
CN13a-CN12d	7H-CC	65.4	G	A			C	C					R	R																	C	C	
CN12d	8H-1, 40	65.8	M	A			C						F	F																	P	C	
CN12d	8H-CC	74.9	G	A									F/C	R																	F	C	
CN12d	9H-CC	84.4	M	C				R					R																			C	
CN12a-c	10H-CC	93.9	G	A				C							R/F	F																	
CN12a-c	11H-CC	103.4	G	C/A											F/C	C/F																	
CN12a	12H-CC	112.9	P	C											C																		
CN12a	13H-CC	122.4	G	A											F/C	C																	
CN12a	14H-CC	131.9	M	A											R/F																		
CN10b-CN10c	15H-CC	137.9	P/M	F/C																	C	R	F										
CN10a?	16X-CC	146.5	P/M	F/C									C								C	R	F										
CN10a-CN9	17X-CC	156.2	G	A																													
CN9b?	18X-CC	165.7	G/M	A											R						C	R	F										
CN9b	19X-CC	175.4	P/M	F/C																	C	R	F										
CN9b	20X-CC	185.0	M/G	A																	C	R	F										
	21X-CC	194.6		B																													
CN9a?	22X-CC	204.3	P	C																	R/F												
	23X-CC	213.9		B																													
	24X-CC	223.5		B																													
CN8-CN9a	25X-1, 118	224.7	P	R																													
	25X-2, 90	225.9		B																													
	25X-3, 102	227.5		B																													
	25X-4, 102	229.0		B																													
	25X-5, 120	230.8		B																													
CN8-CN9a	25X-6, 120	233.2	P	C																													
CN8-CN9a	25X-CC	233.2	P	C											C																		
CN8-CN9a	26X-CC	242.8	P	R/F											C																		
	27X-CC	252.4		B																													
	28X-CC	262.1		B																													
	29X-CC	271.7	P	R																													
CN15	167-1011C-1H-CC	3.3	M	F/C	C/A																												
CN15	2H-CC	12.8	M/G	C	P																												
CN14a	3H-CC	22.3	G	A																													
CN14a	4H-CC	31.8	G	A																													
	5H-CC	41.3	P	R																													
CN13b	6H-CC	50.8	G	A																													
CN13a?	7H-CC	60.3	G	A																													
CN12d	8H-CC	69.8	G	A																													
CN12d	9H-CC	79.3	G	A																													
CN12a-c	10H-CC	88.8	G	A																													
CN12a-b	11H-CC	98.3	P	R																													
CN12a	12H-CC	107.8	G	A																													

Table 5 (continued).

Zone	Core, section, interval (cm)	Depth (mbsf)	Preservation	Abundance	<i>Emiliania huxleyi</i>	<i>Pseudoemiliania lacunosa</i>	<i>Helicosphaera carteri</i>	<i>Helicosphaera sellii</i>	<i>Gephyrocapsa oceanica</i> s.l.	<i>Gephyrocapsa</i> sp. 3	<i>Gephyrocapsa</i> small	<i>Gephyrocapsa</i> large	<i>Discoaster brouweri</i>	<i>Discoaster triradiatus</i>	<i>Discoaster pentaradiatus</i>	<i>Discoaster surculus</i>	<i>Discoaster tamalis</i>	<i>Discoaster asymmetricus</i>	<i>Sphenolithus</i> spp.	<i>Reticulofenestra pseudoumbilicus</i>	<i>Ceratholithus</i> spp.	<i>Ceratholithus telesmus</i>	<i>Ceratholithus acutus</i>	<i>Ceratholithus rugosus</i>	<i>Amaurolithus ampliflicus</i>	<i>Amaurolithus</i> spp.	<i>Discoaster berggrenii/quinquaramus</i>	<i>Minylitha convallis</i>	<i>Coccolithus pelagicus</i>	<i>Calcidiscus macintyrei</i> >11 µm	<i>Calcidiscus leptoporus</i>			
CN12a	13H-CC	117.3	G	A	R	R									F	F	F	F		RR	R	R	F	R	cf					F	C			
CN12a	14H-CC	126.8	G	C/A											F	F	F	F		R	R	R	R/F	R							C	R		
CN10b–CN10c	15H-CC	136.3	P	R/F																C	R													
CN10a–CN9	16X-CC	145.8	P/M	A															R	A														
CN10a–CN9	17X-CC	155.5	P/M	A																A														
CN10a–CN9	18X-CC	165.0	P	A																A														
CN10a–CN9	19X-CC	174.7	P/M	A																A														
CN10a–CN9	20X-CC	189.3	M	A																A														
CN15	167-1011D-1H-CC	7.4	G	A	P	RR	C	R		A																							R	
CN15	2H-CC	16.9	G	C	P		C		R	A																							P	
CN15	167-1011E-1H-CC	5.2	P	F			P		R	P												R												
CN15	2H-CC	14.7	G	A	P		C	C	C	A																								
CN14a	3H-CC	24.2	M/G	A			C	C	C	P																								
CN14a	4H-CC	33.7	G	A			C	C	C	P																								
CN13	5H-CC	43.2	G	A			C	C	C																									
CN13b	6H-CC	52.7	M	C			C	C	C		P																							
CN13a?	7H-CC	62.2	M	C/A			C	C	C																									
CN13a?	8H-CC	71.7	P	F			C	F	R																									
CN12d	9H-CC	81.2	P	C			C																											
CN12	10H-CC	90.7	P	F			F																											
CN12a–c	11H-CC	100.0	M/G	A																														
CN12	12H-CC	109.7	M/G	A																														
CN12a	13H-CC	119.2	P	F		P			F/C																									
CN12	14H-CC	128.0	M/P	C																														
CN12	15H-CC	138.2	M	A																														
CN10c	16H-CC	142.3	P	A																														

Note: See “Explanatory Notes” chapter for abbreviations.

Table 6 (continued).

Core, section, interval	Sample depth (mbsf)	Numeric age (Ma)	Geologic age	Diatom zone	Abundance	Preservation	Environment	Fragmental diatoms	<i>Actinocyclus ehrenbergii</i> var.	<i>Actinocyclus ingens</i>	<i>Actinocyclus ingens ingens</i>	<i>Actinocyclus ingens nodus</i>	<i>Actinocyclus cf. ocellatus</i>	<i>Actinocyclus ochotensis</i>	<i>Actinocyclus tsugaruensis</i>	<i>Actinopychus senarius</i>	<i>Amphora</i> sp.	<i>Aulacosira granulata</i>	<i>Cocconeis californica</i>	<i>Coccinodiscus marginatus</i>	<i>Coccinodiscus marginatus fossilis</i>	<i>Coccinodiscus (Az.) nodulifer</i>	<i>Coccinodiscus</i> sp.	<i>Denticulopsis lauta</i> s.l.	<i>Denticulopsis dimorpha</i>	<i>Denticulopsis hustedii</i>	<i>Denticulopsis hyalina</i>	<i>Denticulopsis katayamae</i>	<i>Denticulopsis praedimorpha</i>	<i>Diploneis smithii</i>
20X-CC	184.3		late Miocene		C	M														F	R			F	F	F		F		
167-1011D-1H-CC	7.4				T	P		R	P																					
167-1011D-2H-CC	16.9				B																									
167-1011E-1H-CC	5.2				B																									
167-1011E-2H-CC	14.7				B																									
167-1011E-3H-CC	24.2				R	P					P														P	P	P		P	
167-1011E-4H-CC	33.7				T	P				P																				
167-1011E-5H-CC	43.2				T	P														P		P								
167-1011E-6H-CC	52.7				T	P														P										
167-1011E-7H-CC	62.2				T	P																								
167-1011E-8H-CC	71.7				T	P																								
167-1011E-9H-CC	81.2				B																									
167-1011E-10H-CC	90.7				R	P		C																						
167-1011E-11H-CC	100.0				R	P																								
167-1011E-12H-CC	109.7				T	P											T													
167-1011E-13H-CC	119.2				T	P																								
167-1011E-14H-CC	128.0				T	P																								
167-1011E-15H-CC	138.2				T	P																								
167-1011E-16H-CC	142.3				B																									

Notes: P = present; more detailed abundance information not available. See "Explanatory Notes" chapter for other abbreviations.

to cool subtropical conditions during the late early through early late Pliocene. The assemblages of late Pliocene through Quaternary age indicate cooler conditions by the nearly consistent abundant occurrence of either or both sinistral and dextral *N. pachyderma*, beginning with Samples 167-1011B-7H-CC and 167-1011C-9H-CC and extending to the top of the sequence. Clear oscillations occur throughout this interval between assemblages dominated by sinistrally or dextrally coiled *N. pachyderma*. This provides evidence for major oscillations in sea-surface temperatures related to glacial/interglacial episodes. We are surprised at the magnitude of the cooling during glacial episodes at the latitude of Site 1011 suggested by the character of the planktonic foraminiferal assemblages. The Pliocene–Quaternary planktonic foraminifer assemblages in Site 1011 also contain distinctly fewer tropical to warm subtropical forms compared with those of Site 1010, indicating much reduced tropical influence.

Benthic foraminifers consistently occur throughout the Pliocene and Quaternary sequence in variable abundances. *Uvigerina* is consistently present. Other taxa that occur more sporadically in samples of this age are *Globobulimina*, *Gyroidina*, *Oridorsalis*, *Cibicides*, *Hoeglundina*, and *Pyrgo*. This assemblage suggests the presence of relatively well-oxygenated bottom water during this interval. Benthic foraminifers are less consistently present in the late Miocene, but most samples contain a small well-preserved assemblage. Agglutinated forms and nodosariids are more conspicuous than in the overlying Pliocene–Quaternary assemblages, and there is a suggestion of lower oxygenation of the benthic environment.

Calcareous Nannofossils

Nannofossils are generally common to abundant and well-preserved through the Quaternary and Pliocene, but the preservation is poor and several samples are barren in the late Miocene. A time interval spanning late Miocene Zone CN9a–CN8 to late Pleistocene Zone CN15 (Okada and Bukry, 1980) was recognized in Hole 1011B (Table 5). The lowest zone recorded in Hole 1011C is Zone CN10a–CN9. Hole 1011E represents an interval ranging from the lower Pliocene Zone CN10 to the late Pleistocene CN 15.

In the Quaternary, nannofossil assemblages are marked by the presence of *Emiliania huxleyi*, *Pseudoemiliania lacunosa*, *Calcidiscus leptoporus*, *Helicosphaera carteri*, and several morphotypes of *Gephyrocapsa* spp. and *Ceratolithoides* spp.

The Pliocene/Pleistocene boundary is placed by the FO of *Gephyrocapsa oceanica* s.l. Pliocene nannofossil assemblages are marked by an association of *Helicosphaera carteri*, *Discoaster brouweri*, *Discoaster tamalis*, *Discoaster pentaradiatus*, *Discoaster surculus*, *Amaurolithus delicatus*, and several morphotypes of *Reticulofenestra* and *Ceratolithus*. The upper/lower Pliocene boundary is recognized close to the LO of *Reticulofenestra pseudoumbilicus* (base of CN12a), and occurs between Samples 167-1011B-14H-CC and 15H-CC, between 167-1011C-14H-CC and 15H-CC, and between 167-1011E-15H-CC and 16H-CC. Presence of *Amaurolithus* spp. and *Ceratolithus acutus* allows assignment of the lower Pliocene to Zone CN10c/CN10b. The Miocene/Pliocene boundary was placed between Samples 167-1011B-17X-CC and 18X-CC by the LO of *Discoaster quinqueramus/berggrenii*. The co-occurrence of *Discoaster quinqueramus/berggrenii* and *Amaurolithus* spp. in Samples 167-1011B-18X-CC to 167-1011B-23X-CC allows the assignment of this interval to Zone CN9b. In Hole 1011C, the Miocene/Pliocene boundary was not recognized because *Discoaster quinqueramus/berggrenii* is absent. In the interval, calcareous nannofossils are strongly etched and a precise biostratigraphic assignment is difficult. Only a few specimens of *Minylitha convallis*, which is characteristic of Zones CN8 and CN9a, were observed in sediments between Samples 167-1011B-25X-1, 118 cm, and 167-1011B-26X-CC.

Diatoms

Diatoms are abundant to common and display excellent to good preservation in the lowermost nine cores of Hole 1011B (194.6 to 271.7 mbsf). Above 185 mbsf in all holes, throughout the uppermost Miocene to Quaternary, diatoms are few to barren, and large quantities of clay, clastic material, and calcareous nannofossils continuously dominate the lithostratigraphic succession.

Diatom assemblages are typical of the subarctic region of the north Pacific and can be zoned readily using the Leg 167 north Pacific diatom zonation (Table 6). Assemblages examined from Samples 167-1011B-21X-CC through 26X-CC are commonly dominated by *Coscinodiscus marginatus*, a large, robust centric diatom that is resistant to dissolution. This horizon falls just below Core 167-1011C-20X.

A complete sequence from the *Thalassionema schraderi* Zone (NPD 6b) to the *Denticulopsis dimorpha* Zone (NPD 5d) was recovered through Samples 167-1011B-21X-CC to 29X-CC, and wholly fall within the middle late Miocene (~7.1–9.8 Ma; Tables 6, 7). The LCO of the *Denticulopsis hustedtii* group involving *Denticulopsis katayamae* in Sample 167-1011B-27X-CC marks the boundary between the *Thalassionema schraderi* Zone (NPD 6b) and the underlying *Denticulopsis katayamae* Zone (NPD 6a). The top of the *Denticulopsis dimorpha* Zone (NPD 5d) has been placed between Samples 167-1011B-27X-CC and 28X-CC by the LO of *D. dimorpha*. The presence of *D. dimorpha* in Sample 167-1011B-29X-CC indicates that the base of the cored section at Site 1011 may be younger than 9.8 Ma, an assignment that is more consistent with that of the radiolarians (Tables 6, 7).

Persistent reworking of middle Miocene forms of *D. hustedtii* and *D. dimorpha* occur in the Pliocene and Quaternary. The Pliocene–Quaternary assemblages are dominated by cold-water *Neodenticula* species of middle-to-high latitudes (Akiba, 1986; Koizumi and Tanimura, 1985; Barron, 1992). The scarcity of diatoms in the clay-rich, upper part of the sequence in Sites 1010 and 1011 results from ecological exclusion from the relatively warm coastal waters or dissolution.

Radiolarians

Rare and poorly preserved radiolarians were found in the sediments of the upper lithostratigraphic Unit I of Quaternary age. Rare to few representatives of radiolarians were recognized in the lithostratigraphic Unit II. Rare to abundant and well-preserved radiolarians occur in the lower lithostratigraphic Unit III of late Miocene age. Assemblages of this site are made up of mid-latitude and Arctic species. Tropical forms were not found. Common to abundant species indicative of upwelling areas such as *Collosphaera huxleyi*, *Eucyrtidium erythromystax*, and *Phormostichoartus crustula* suggest a persistent upwelling system during the late Miocene to early Pleistocene at this Site (Tables 8, 9).

Presence of morphotypes transitional between *Lamprocyrtis nigriinae* and *L. neoheteroporos* gives an early Pleistocene age (1.2 to 0.9 Ma) to Sample 167-1011B-3H-CC (27.4 mbsf). Samples 1011B-1H-CC to 3H-CC (8.4 to 27.4 mbsf) are thus placed in the *B. aquilonaris* and *S. universus* Zones, although the LO of *E. matuyamai* at 1.0 Ma was not observed. Samples 167-1011B-4H-CC to 13H-CC (55.9 to 122.4 mbsf) are tentatively placed in the *E. matuyamai* and *S. langii* Zones since consistent occurrence of *S. peregrina* was not observed. Consistent occurrence of *S. peregrina* places the interval between Samples 167-1011B-18X-CC and 23X-CC (165.7 to 213.9 mbsf) in the late Miocene to early Pliocene *S. peregrina* Zone. The evolutionary transition between *S. delmontensis* and *S. peregrina*, which indicates the base of the *S. peregrina* Zone, was observed in Sample 167-1011B-

Table 8. Range of stratigraphically important radiolarians in Hole 1011B.

Zone	Core, section, interval	Depth (mbsf)	Abundance	Preservation	<i>Anthocyrtidium ehrenbergi</i>	<i>Anthocyrtidium nosicae</i>	<i>Anthocyrtidium pliocenica</i>	<i>Bostryocella cribrosa</i>	<i>Bostryostrobilus aquilonaris</i>	<i>Bostryostrobilus bramlettei</i>	<i>Bostryostrobilus praetunidulatus</i>	<i>Circodiscus ellipticus</i>	<i>Collosphaera huxleyi</i>	<i>Cycladophora bicincta</i>	<i>Cycladophora cosma</i>	<i>Cycladophora davisiana davisiana</i>	<i>Cyrtocapsella cornuta</i>	<i>Cyrtocapsella japonica</i>	<i>Diartus hughesi</i>	<i>Dicryophimus splendens</i>	<i>Didymocyrtis antepenultima</i>	<i>Eucyrtidium calvertense</i>	<i>Eucyrtidium inflatum</i>
<i>B. aquilonaris</i> + <i>S. universus</i>	167-1011B-1H-CC	8.40	R	P																			
	2H-CC	17.40	R	R																			
	3H-CC	27.40	R	G					P							P							
<i>E. matuyamai</i> + <i>S. langii</i>	4H-CC	55.90	F	G					P							P							
	5H-CC	46.40	R	P												P							
	6H-CC	55.90	R	P																			
	7H-CC	49.60	F	G					P							P							
	8H-CC	74.90	F	G					P														
	9H-CC	84.40	R	M					P														
	10H-CC	93.90	R	P																			
	11H-CC	103.40	C	M		P			P									P					
	12H-CC	112.90	R	P					P														
	13H-CC	122.40	B	P																			
Unzoned	14H-CC	131.90	R	P			P			P													P
	15H-CC	137.90	B																				
	16X-CC	145.60	B																				
	17X-CC	156.20	B																				
	18X-CC	165.70	F	M						P													
<i>S. peregrina</i>	19X-CC	175.40	C	M						P													
	20X-CC	185.00	A	G						P								P					P
	21X-CC	194.60	A	G				P	P														
	22X-CC	204.30	A	G				P		P													
	23X-CC	213.90	A	G						P	P		P										
<i>D. penultima</i>	24X-CC	223.50	A	G						P	P	P											P
	25X-CC	233.20	A	G						P	P												P
	26X-CC	242.80	A	G	P								P										P
	27X-CC	252.40	A	G																			
<i>D. antepenultima</i>	28X-CC	262.10	A	G							P							P		P			P
	29X-CC	271.70	A	G						P							P	P		P			P

Notes: P = present; more detailed abundance information not available. See "Explanatory Notes" chapter for other abbreviations.

23X-CC (213.9 mbsf). The base of the *D. penultima* Zone (late Miocene) is well defined by the FO of *D. hughesi* in Sample 167-1011B-28X-CC (262.1 mbsf). Samples 167-1011B-28X-CC and 167-1011B-29X-CC are placed in the *D. antepenultima* Zone since *D. petterssoni* was not found. Occurrence of rare representatives of *C. cornuta* within this interval are interpreted as reworking. The LO of *L. n. magnacornuta* at 8.8 Ma is also located in this interval. The interval between 1011C-11H-CC and 14-CC (98.3 to 126.8 mbsf) is tentatively placed in the early Pleistocene *E. matuyamai* and *S. langii* Zones as indicated by the presence of *Lamprocyrtis neoheteroporos*, *L. heteroporos*, and *S. universus*. The interval between Samples 167-1011C-18H-CC and 20H-CC (165 to 184.3 mbsf) was placed in the *S. peregrina* Zone, based on the presence of rare and poorly to well-preserved *S. peregrina* and the absence of *L. neoheteroporos*.

**PALEOMAGNETISM
Laboratory Procedures**

We measured the remanent magnetization of archive halves of APC cores from Site 1011 with the pass-through cryogenic magnetometer. After measuring natural remanent magnetization (NRM), 15 cores from Hole 1011B were demagnetized with a peak alternating field (AF) of 20 mT. Because the demagnetization at 20 mT reduced the magnetic intensity of most sections in Hole 1011B to less than 1 mA/m, we demagnetized four APC cores from the topmost part of Hole 1011C at 10 mT AF. A few discrete samples from Hole 1011B were stepwise AF demagnetized using the Schonstedt Alternating

Field Demagnetizer (GSD-1) and measured with the Minispin magnetometer.

Results and Discussion

The NRM intensity of the APC cores from Hole 1011B was on the order of 10 mA/m in most cores (Fig. 9). The direction of NRM is inclined steeply downward with declinations around 0°. This component suggests a drilling-induced remanence, as noticed already at the previous site (see "Paleomagnetism" section, "Site 1010" chapter, this volume). After AF demagnetization at 20 mT, the magnetic intensities were reduced to about 10% of their NRM values, and the inclinations became shallower. Stepwise AF demagnetization of five discrete samples showed that the almost vertical component resides in the coercivity range mostly below 5 mT (Fig. 10).

Although the bulk of the drilling-induced remanence was removed by AF demagnetization, a magnetostratigraphy could not be determined for Hole 1011B from the magnetic inclinations (Fig. 9). According to the nannofossil and planktonic foraminiferal biostratigraphy, the Pleistocene/Pliocene boundary is located at about 50 mbsf (see "Biostratigraphy" section, this chapter). This suggests that an interval above 50 mbsf should correspond to Chron C1r. Cores 1H to 5H, however, had positive inclinations except for a few dispersed horizons with negative inclinations. Below 50 mbsf, a few short reversely magnetized horizons were found at around 56, 72, 74, 82, and 121 mbsf. These data suggest deposition during reversed polarity chrons, but the few reversals are not sufficient to be correlated to the standard polarity time scale.

Table 8 (continued).

Zone	Core, section, interval	Depth (mbsf)	Abundance	Preservation	<i>Gondwanaria dogieli</i>	<i>Lamprocyrtis neoheteroporos</i>	<i>Lamprocyrtis nigrinae</i>	<i>Larospira moschkovskii</i>	<i>Lychnocanoma n. sakai</i>	<i>Lychnocanoma nipponica magnicornuta</i>	<i>Lychnocanoma nipponica nipponica</i>	<i>Phormostichocartus crustula</i>	<i>Prunopyle hayesi</i>	<i>Sphaeropyle langii</i>	<i>Sphaeropyle robusta</i>	<i>Spirema circularis</i>	<i>Stauraxiphos communis</i>	<i>Stichocorys delmontensis</i>	<i>Stichocorys peregrina</i>	<i>Sylocaontarium acqulionium</i>	<i>Stylatractus universus</i>	<i>Sylodictya validispina</i>	<i>Theocorys redondoensis</i>
<i>B. aquilonaris</i> +	167-1011B-1H-CC	8.40	R	P																			
	2H-CC	17.40	R	P																			
<i>S. universus</i>	3H-CC	27.40	R	G	P	P																	
	4H-CC	55.90	F	G					P					P							P		
<i>E. matuyamai</i> +	5H-CC	46.40	R	P																			
	6H-CC	55.90	R	P																			
<i>S. langii</i>	7H-CC	49.60	F	G					P												P		
	8H-CC	74.90	F	G			P														P		
	9H-CC	84.40	R	M			P														P		
	10H-CC	93.90	R	P																	P		
	11H-CC	103.40	C	M			P														P	P	P
	12H-CC	112.90	R	P			P														P	P	P
Unzoned	13H-CC	122.40	B	P			P														P		
	14H-CC	131.90	R	P						P											P		
	15H-CC	137.90	B																				
	16X-CC	145.60	B																				
	17X-CC	156.20	B																				
	18X-CC	165.70	F	M																	P	P	
<i>S. peregrina</i>	19X-CC	175.40	C	M											P						P	P	
	20X-CC	185.00	A	G	P					P	P				P						P	P	
	21X-CC	194.60	A	G						P	P				P						P	P	
	22X-CC	204.30	A	G	P					P	P	P			P						P	P	
	23X-CC	213.90	A	G	P					P	P				P						P	P	
	24X-CC	223.50	A	G						P	P						P	P			P	P	
<i>D. penultima</i>	25X-CC	233.20	A	G	P					P	P	P									P	P	
	26X-CC	242.80	A	G						P	P	P			P	P					P	P	P
<i>D. antepenultima</i>	27X-CC	252.40	A	G								P									P	P	P
	28X-CC	262.10	A	G																	P	P	P
	29X-CC	271.70	A	G	P					P	P	P									P	P	P

An interesting feature of the paleomagnetic data at Site 1011 is the steplike reduction in magnetic intensity from 1.5 to 2.5 mbsf (Fig. 11). The intensity drop of remanent magnetization corresponds to a decrease in magnetic susceptibility in the same interval (see “Physical Properties” section, this chapter; Fig. 11), because of a strong decrease in concentration of magnetic minerals within one meter. The destruction of fine magnetic minerals has often been reported for continental margin sediments characterized by high sedimentation rate and high organic matter content; the cause has been attributed to diagenetic change of magnetite with sulfate reduction (e.g., Karlin and Levi, 1983; Canfield and Berner, 1987). Leslie et al. (1990) and Lund et al. (1992) demonstrated that dissolution of magnetic material occurs in the deep basins of the California Borderland where the water depths range between 500 and 1500 m. Our data suggest that similar diagenetic processes possibly occur in the Animal Basin at a depth of 2000 m, explaining the unclear magnetostratigraphy at Site 1011.

COMPOSITE DEPTHS AND SEDIMENTATION RATES

Multisensor track (MST) data, collected at 4- to 6-cm intervals from Holes 1011A through 1011E, and color reflectance data, collected at 6-cm intervals from Holes 1011B and 1011C, were used to determine depth offsets in the composite section. On the composite depth scale (expressed as mcd, meters composite depth), features of the plotted MST and color reflectance data present in adjacent holes

are aligned so that they occur at approximately the same depth. Working from the top of the sedimentary sequence, a constant was added to the mbsf (meters below seafloor) depth for each core in each hole to arrive at a mcd depth for that core. The depths offsets that compose the composite depth section are given in Table 10 (also on CD-ROM, back pocket, this volume). Continuity of the sedimentary sequence was documented only for the upper 150 mcd. Below about 150 mcd, the cores were placed into composite depth, but continuity could not be verified.

Magnetic susceptibility was the primary parameter used for inter-hole correlation purposes. Color reflectance measurements and GRAPE bulk density were used in a few intervals, particularly at the bottom of the section to provide additional support for composite construction. Natural gamma-ray activity measurements were made throughout the entire section at all holes, but the sampling intervals of 12–15 cm were insufficient for interhole correlation.

The magnetic susceptibility, color reflectance, and GRAPE bulk density records used to verify core overlap for Site 1011 are shown on a composite depth scale in Figures 12, 13, and 14, respectively. The cores from Holes 1011B and 1011C provide continuous overlap to about 150 mcd. The composite records suggest that up to 2 m of material is missing between cores in all holes down to about 150 mcd. As there are no data to fill possible core gaps below Cores 167-1011B-15H, 1011C-15H, and 1011E-15H, an assessment of core gap length below about 150 mcd is not possible.

Following construction of the composite depth section for Site 1011, a single spliced record was assembled from the aligned cores.

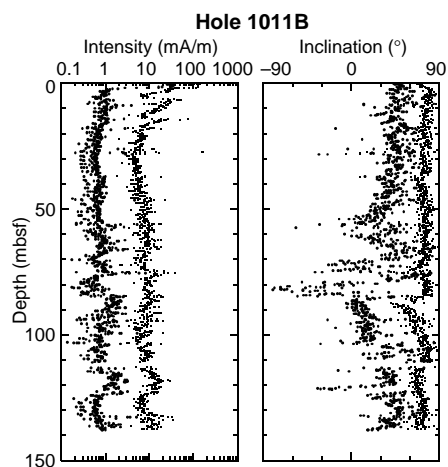


Figure 9. Plots of magnetic intensity and inclination of cores from Hole 1011B. Small and large dots represent magnetic intensity and inclination before and after AF demagnetization at 20 mT, respectively.

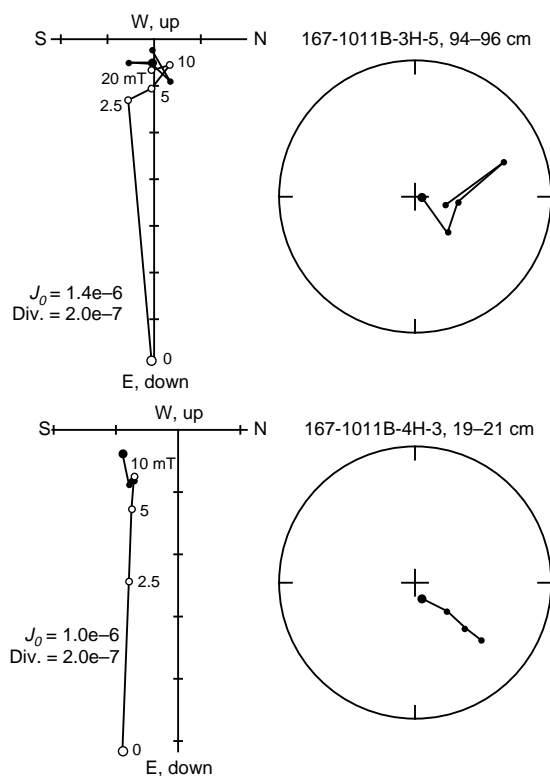


Figure 10. Orthogonal vector projection (left) and equal-area projection (right) of AF demagnetization of two discrete samples of normal polarity. The intensity of magnetization decreases rapidly when a 10 mT AF is applied. J_0 is the magnetization before AF treatment.

mbsf to 31.6 mM at 136.35 mbsf, then increase to 44.9 mM at 247.25 mbsf. The decrease in dissolved calcium in the upper sediment is coincident with the sulfate decrease and the alkalinity increase from sulfate reduction. This, combined with the nonlinear relationship of calcium and magnesium, suggests that authigenic mineral precipitation may be significant in influencing these profiles. Lithium concentrations increase to a broad maximum around 100 μM from 110 to 160

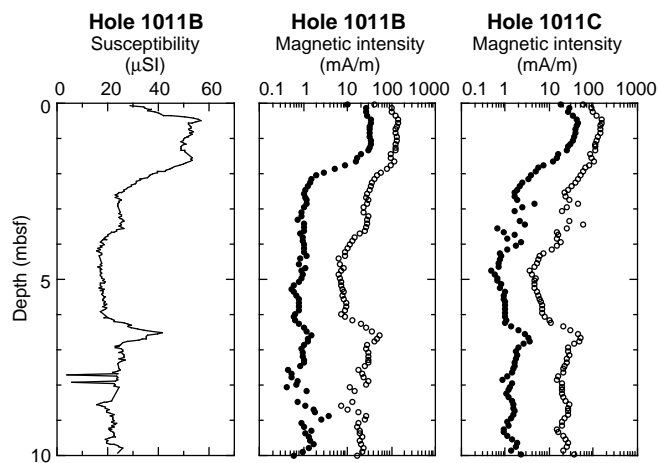


Figure 11. Comparison of the intensity of magnetization before (open circles) and after AF demagnetization (solid symbols) in the upper 10 mbsf of Holes 1011B and 1011C. Magnetic susceptibility (left) shows a similar depth dependence to magnetic intensity, dropping sharply between 1.5 and 2.5 mbsf.

m, then decrease to 39 μM at 247.25 mbsf (Fig. 17). Potassium concentrations increase slightly to 13.1 mM at 31.85 mbsf, then generally decrease with increasing depth.

ORGANIC GEOCHEMISTRY

We measured elemental compositions and volatile hydrocarbons of sediments from Site 1011 (for methods see “Organic Geochemistry” section, “Explanatory Notes” chapter, this volume).

Volatile Hydrocarbons

Concentrations of methane, ethane, and propane were routinely monitored at Hole 1011B according to shipboard safety and pollution prevention considerations. The results are displayed in Figure 18 and Table 14. Between 0 and 41 mbsf headspace methane concentration is near the detection limit of the HP 5890 gas chromatograph. At about 41 mbsf the concentration increases rapidly, reaching a maximum value of 6347 ppm at 89 mbsf, and decreases again to near zero at about 150 mbsf. One single sample at 190 mbsf displayed a higher concentration (2505 ppm). No significant amounts of higher molecular weight hydrocarbons were observed, indicating that the methane was derived from biogenic organic matter degradation and is not significant for safety and pollution investigations.

Elemental Analysis

The concentrations of inorganic carbon, total carbon, total nitrogen, and total sulfur are presented in Table 15 (also on CD-ROM, back pocket) and Figure 19.

The percentage of calcium carbonate (CaCO_3) was calculated from the inorganic carbon concentrations by assuming that all carbonate occurs in the form of calcite. The concentration of CaCO_3 varies between 0 and 60 wt% and depends on lithology. Lithostratigraphy Unit I, Subunits IIIA and IIIB, and Unit IV (see “Lithostratigraphy” section, this chapter) generally show low carbonate concentrations, while Subunits IIA and IIB are characterized by higher values. High CaCO_3 contents of Subunit IIA coincide with abundant well-preserved nannofossils (see “Biostratigraphy” section, this chapter). Compared to Subunit IIA, CaCO_3 contents are lower in Subunit IIB and display a higher ampli-

Table 10. Site 1011 composite depth section.

Core, section	Depth (mbsf)	Offset (m)	Depth (mcd)
167-1011A-1H-1	1.9	-0.34	1.56
167-1011B-1H-1	0	0	0
2H-1	8.4	0.53	8.93
3H-1	17.9	3.24	21.14
4H-1	27.4	4.04	31.44
5H-1	36.9	4.58	41.48
6H-1	46.4	5.28	51.68
7H-1	55.9	6.52	62.42
8H-1	65.4	6.32	71.72
9H-1	74.9	6.22	81.12
10H-1	84.4	6.92	91.32
11H-1	93.9	7.04	100.94
12H-1	103.4	8.24	111.64
13H-1	112.9	8.96	121.86
14H-1	122.4	10.3	132.7
15H-1	131.9	10.94	142.84
16X-1	137.9	10.94	148.84
17X-1	146.5	10.56	157.06
18X-1	156.2	10.56	166.76
19X-1	165.7	12.12	177.82
20X-1	175.4	14.44	189.84
21X-1	185	14.44	199.44
22X-1	194.6	14.44	209.04
23X-1	204.3	14.44	218.74
24X-1	213.9	14.44	228.34
25X-1	223.5	14.44	237.94
26X-1	233.2	14.44	247.64
27X-1	242.8	14.44	257.24
28X-1	252.4	14.44	266.84
167-1011C-1H-1	0	0	0
2H-1	3.3	-0.07	3.23
3H-1	12.8	0.6	13.4
4H-1	22.3	2.43	24.73
5H-1	31.8	3.76	35.56
6H-1	41.3	4.13	45.43
7H-1	50.8	5.7	56.5
8H-1	60.3	6.84	67.14
9H-1	69.8	7.76	77.56
10H-1	79.3	8.1	87.4
11H-1	88.8	9.06	97.86
12H-1	98.3	9.98	108.28
13H-1	107.8	10.9	118.7
14H-1	117.3	11.26	128.56
15H-1	126.8	12.72	139.52
16X-1	136.3	12.42	148.72
17X-1	145.8	12.52	158.32
18X-1	155.5	12.56	168.06
19X-1	165	12.46	177.46
20X-1	174.7	12.5	187.2
167-1011D-1H-1	0	0.15	0.15
2H-1	7.4	0.61	8.01
167-1011E-1H-1	0	0.15	0.15
2H-1	5.2	0.33	5.53
3H-1	14.7	1.8	16.5
4H-1	24.2	2.13	26.33
5H-1	33.7	3.22	36.92
6H-1	43.2	3.42	46.62
7H-1	52.7	4.31	57.01
8H-1	62.2	4.76	66.96
9H-1	71.7	4.89	76.59
10H-1	81.2	4.3	85.5
11H-1	90.7	5.3	96
12H-1	100.2	6.17	106.37
13H-1	109.7	6.59	116.29
14H-1	119.2	7.61	126.81
15H-1	128.7	9.06	137.76
16H-1	138.13	10.72	148.85

Note: This table is also on CD-ROM, back pocket, this volume.

tude variation. This is probably the result of increased carbonate dissolution, as indicated by strongly corroded calcareous microfossils (see "Biostratigraphy" section, this chapter).

Organic carbon concentrations are generally high throughout the sediment column, varying with high amplitude between 0.5 and 2.5 wt% (Table 15; Fig. 19). Some single spikes of up to 6 wt% occur. Variation of organic carbon occurs on a meter scale which is also vis-

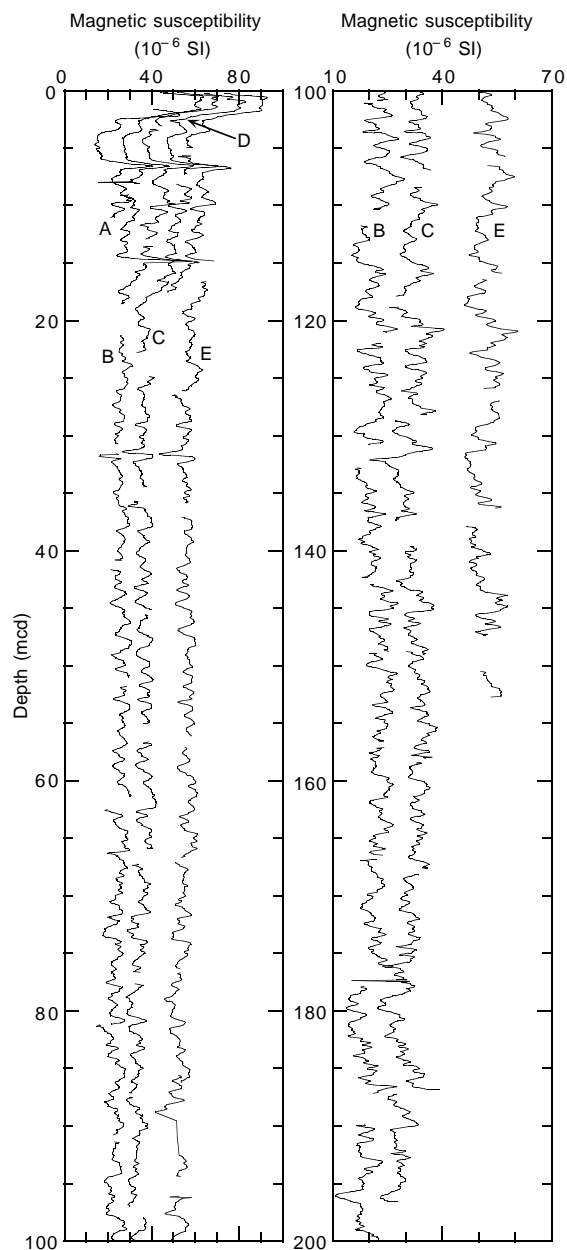


Figure 12. Smoothed (30-cm Gaussian) magnetic susceptibility data for the upper 200 m from Site 1011 on the mcd scale. Holes 1011A through 1011E are offset from each other by a constant (10×10^{-6} SI).

ible in the color of the sediment. Dark greenish intervals display higher organic carbon contents, whereas lighter intervals are carbonate rich and organic-carbon lean. Further detailed investigations on the quality of the organic matter will shed light on whether these sedimentary cycles correlate changes in the composition of organic carbon.

Total nitrogen values at Site 1011 vary between 0.04 and 0.39 wt%. Total sulfur content ranges from 0 to about 3.5 wt% (Table 15). The majority of sulfur occurs as authigenic pyrite, which is finely disseminated in the sediment (see "Lithostratigraphy" section, this chapter).

Total organic carbon/total nitrogen ratios were used to characterize the type of organic matter in the sediments. Most of the TOC/TN values are below 12, indicating a predominance of marine organic matter (Figs. 19, 20; Bordovskiy, 1965; Emerson and Hedges, 1988).

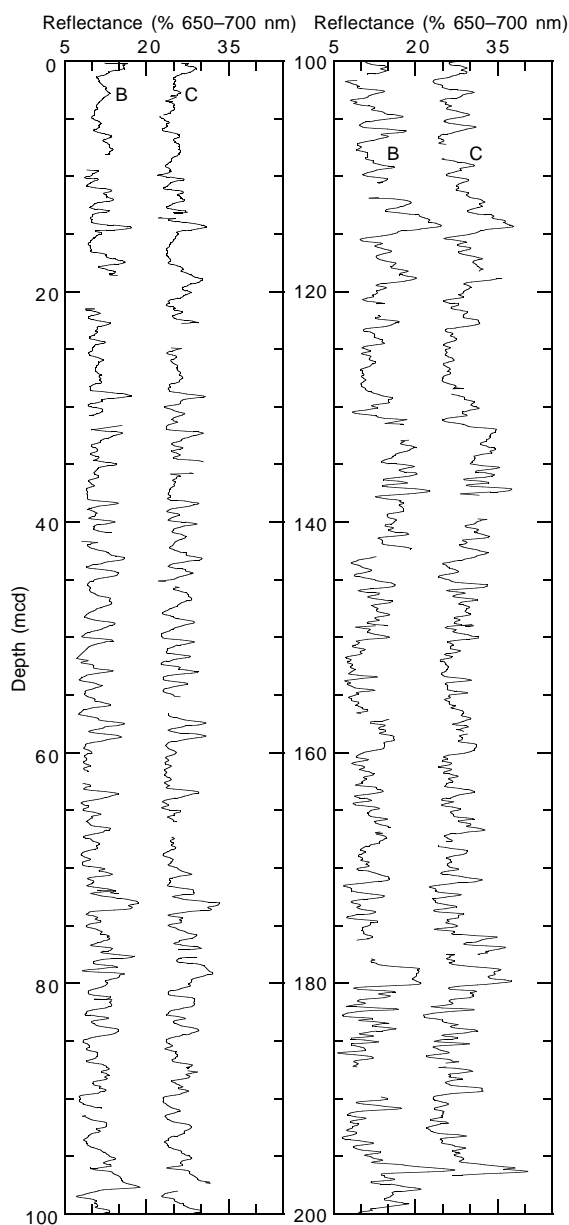


Figure 13. Smoothed (30-cm Gaussian) color reflectance (% 650–700 nm band) data for the upper 200 m from Site 1011 on the mcd scale. Holes 1011B and 1011C are offset from each other by a constant (10%).

A positive correlation between total organic carbon and TOC/TN ratio (Fig. 21) indicates that episodic supply of terrigenous organic matter likely resulted in enhanced TOC values. Estimates of the amounts of marine and terrestrial organic carbon still have to be confirmed by shore-based elemental and microscope analyses.

PHYSICAL PROPERTIES

Multisensor Track Measurements

The shipboard physical properties program at Site 1011 included nondestructive measurements of GRAPE bulk density, magnetic susceptibility, *P*-wave velocity, and natural gamma-ray activity on whole sections of all cores using the MST (Fig. 22). Magnetic susceptibility was measured at 2-cm intervals at low sensitivity (1-s measuring time). GRAPE and PWL measurements were measured at

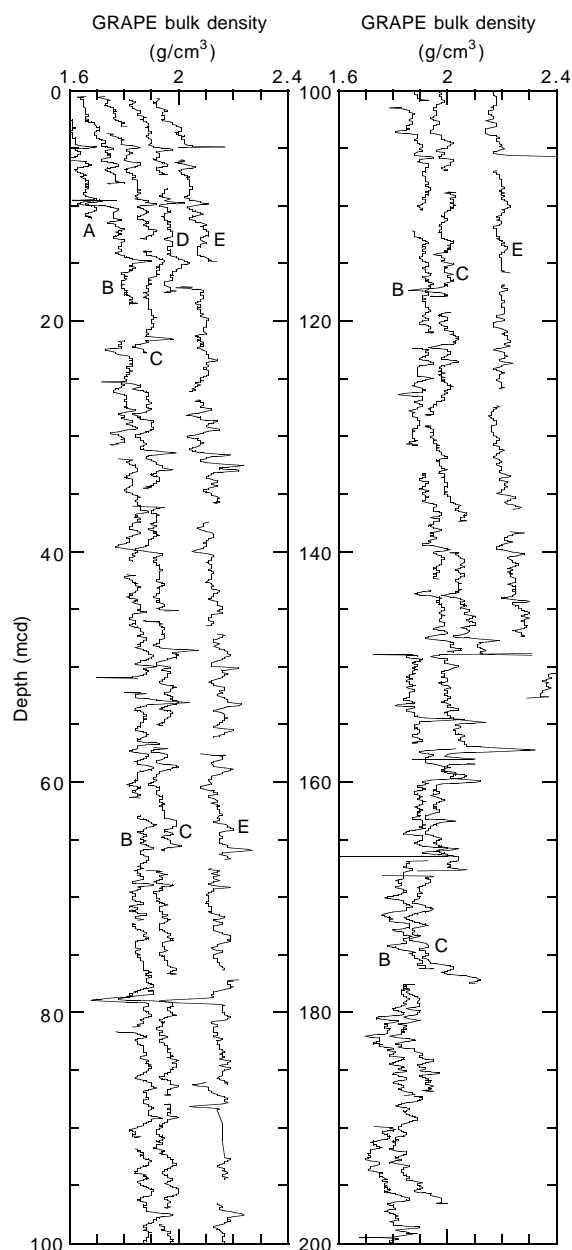


Figure 14. Smoothed (30-cm Gaussian) GRAPE data for the upper 200 m from Site 1011 on the mcd scale. Holes 1011A through 1011E are offset from each other by a constant (0.1 g/cm³).

2-cm intervals for bulk density and velocity, respectively. Natural gamma-ray activity was measured with a 10-s count every 12 cm.

Index Properties

Index properties measurements were made, on average, at one sample per working section in all cores of Hole 1011B and one sample every 10 cm in Core 167-1011E-13H for a high-resolution calibration study of shipboard porosity with the downhole logging data. Samples usually were taken at intervals where color reflectivity measurements were made and where samples were collected for calcium carbonate analysis with the objective of determining mass accumulation rates. Index properties were determined by the gravimetric method using Method C (see “Explanatory Notes” chapter, this volume). Index property data are presented in Table 16 on CD-ROM in the

Table 11. Site 1011 splice tie points.

Hole, core, section, interval (cm)	Depth		Hole, core, section, interval (cm)	Depth	
	(mbsf)	mcd		(mbsf)	mcd
1011B-1H-5, 52	6.52	6.52	tie to 1011B-1H-1, 0	0	0.00
1011C-2H-5, 95	10.25	10.18	tie to 1011C-2H-3, 29	6.59	6.52
1011B-2H-4, 82	13.72	14.25	tie to 1011B-2H-1, 125	9.65	10.18
1011C-3H-6, 91	21.21	21.81	tie to 1011C-3H-1, 85	13.65	14.25
1011B-3H-6, 43	25.83	29.07	tie to 1011B-3H-1, 67	18.57	21.81
1011C-4H-6, 7	29.87	32.30	tie to 1011C-4H-3, 134	26.64	29.07
1011B-4H-5, 83	34.23	38.27	tie to 1011B-4H-1, 86	28.26	32.30
1011C-5H-6, 63	39.93	43.69	tie to 1011C-5H-2, 121	34.51	38.27
1011B-5H-6, 99	45.39	49.97	tie to 1011B-5H-2, 71	39.11	43.69
1011C-6H-6, 31	49.16	53.29	tie to 1011C-6H-3, 149	45.84	49.97
1011B-6H-6, 139	55.29	60.57	tie to 1011B-6H-2, 11	48.01	53.29
1011C-7H-5, 91	57.71	63.41	tie to 1011C-7H-3, 107	54.87	60.57
1011B-7H-7, 11	65.01	71.53	tie to 1011B-7H-1, 99	56.89	63.41
1011C-8H-6, 139	69.19	76.03	tie to 1011C-8H-3, 139	64.69	71.53
1011B-8H-7, 15	74.55	80.87	tie to 1011B-8H-3, 131	69.71	76.03
1011C-9H-5, 31	76.11	83.87	tie to 1011C-9H-3, 31	73.11	80.87
1011B-9H-6, 139	83.79	90.01	tie to 1011B-9H-2, 125	77.65	83.87
1011C-10H-5, 119	86.49	94.59	tie to 1011C-10H-2, 111	81.91	90.01
1011B-10H-5, 143	91.83	98.75	tie to 1011B-10H-3, 27	87.67	94.59
1011C-11H-4, 135	94.65	103.71	tie to 1011C-11H-1, 89	89.69	98.75
1011B-11H-6, 71	102.11	109.15	tie to 1011B-11H-2, 127	96.67	103.71
1011C-12H-3, 87	102.17	112.15	tie to 1011C-12H-1, 87	99.17	109.15
1011B-12H-6, 51	111.41	119.65	tie to 1011B-12H-1, 51	103.91	112.15
1011C-13H-3, 63	111.43	122.33	tie to 1011C-13H-1, 95	108.75	119.65
1011B-13H-6, 115	121.55	130.51	tie to 1011B-13H-1, 47	113.37	122.33
1011C-14H-4, 75	122.55	133.81	tie to 1011C-14H-2, 45	119.25	130.51
1011B-14H-5, 123	129.63	139.93	tie to 1011B-14H-1, 111	123.51	133.81
1011C-15H-7, 51	136.31	149.03	tie to 1011C-15H-1, 41	127.21	139.93

Note: This table is also on CD-ROM, back pocket, this volume.

Table 12. Site 1011 sedimentation rate age control points.

Event	Depth (mcd)	Age (Ma)
<i>T. P. lacunosa</i>	20.897	0.460
B large <i>Gephyrocapsa</i> spp.	60.343	1.440
<i>T. D. pentaradiatus</i>	92.673	2.500
<i>T. R. pseudoumbilicus</i> , <i>B. C. acutus</i>	145.773	4.385
<i>T. D. quinqueramus</i>	167.040	5.560
LCO <i>D. hustedtii</i>	252.440	8.600
<i>T. D. dimorpha</i>	271.690	9.160

Note: T = top, B = bottom, LCO = last common occurrence.

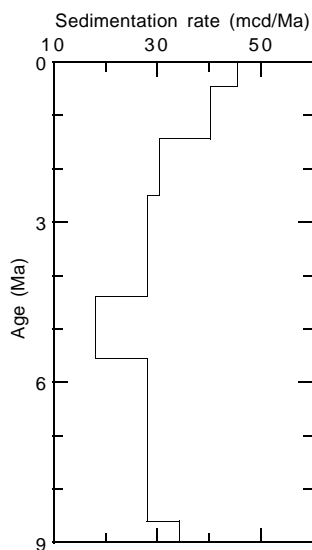


Figure 15. Sedimentation rate vs. age based on the age control points from Table 12.

back pocket of this volume. Uncorrected GRAPE density and index property density produce remarkably similar trends (Fig. 23). Below 138 mbsf, where coring switched from APC to XCB, the uncorrected GRAPE values are lower than the index property density values, most likely because of the addition of drilling slurry lowering the measured density. In addition to bulk density, the index properties of void ratio, porosity, water content, dry-bulk density, and grain density were determined (Fig. 24). Notice that at about 204 mbsf the grain density values drop from about 2.7 to 2.5 g/cm³, reflecting a transition from calcareous nannofossil-rich sediments to more siliceous diatom- and radiolarian-rich sediments, marking the boundary between lithostratigraphic Units II and III (“Lithostratigraphy” section, this chapter).

Compressional-Wave Velocity

P-wave velocity measurements were made, on average, once per section in Hole 1011B. The sonic transducer pair of the digital sound velocimeter (pair T1), which are inserted parallel to the core axis (z-direction), were used to a depth of only 26 mbsf in Hole 1011B. The sediment is too consolidated below this depth to use insertable transducers, so the Hamilton Frame (pair T3) was used for sonic measurements in the x-direction while the core was still in the liner. Velocity values (Table 17 on CD-ROM in the back pocket of this volume) show an inverse correlation with porosity values (Fig. 25). Discrete values of velocity show a marked shift to higher values when the digital sound velocimeter tools were changed from insertable (T1) to Hamilton Frame (T3) (Fig. 26). This most likely corresponds to the added pressure generally required to produce a detectable signal.

Heat Flow

Thermal conductivity was measured in the sediment cores of Hole 1011C (Table 18 on CD-ROM in the back pocket of this volume) about every 2 m down to 107.8 mbsf. Five good-quality measurements were made in Hole 1011C: 5.3°C at 31.8 mbsf, 8.1°C at 50.8 mbsf, 9.6°C at 69.8 mbsf, 11.8°C at 88.8 mbsf, and 14.3°C at 107.8 mbsf in Cores 167-1011C-4H, 6H, 8H, 10H, and 12H, respectively (Fig. 27). In addition to these data, the bottom-water temperature was measured during the run for Core 167-1011C-4H, leaving the tool at the mudline for approximately 12.6 min before piston coring. The data indicate a bottom-water temperature of 2.7°C ± 0.1°C. The six data points yield a thermal gradient of 108°C/km (Fig. 28). Using an average measured thermal conductivity of 1.023 W/(m·K) provides a heat-flow estimate of 111 mW/m² at Site 1011.

Color Reflectance

In general, color reflectance values average 10%, significantly lower than at Site 1010. This is primarily the result of a higher terrigenous component at Site 1011. Despite this dilution effect, cyclical variations in microfossil content were detected throughout the section. Nannofossils appear to be the primary agent of color change in lithostratigraphic Unit II, whereas diatoms are predominant in lithostratigraphic Unit III. Data from 25 to 70 mbsf (lithostratigraphic Unit II) of Hole 1011C are presented in Figure 29A. Nannofossil-enriched clays in this section have color reflectance values ranging from 10% to 15% and a broad spectral peak from 500 to 600 nm (Fig. 29B), whereas more barren clays have lower reflectance levels (5% to 10%) and a flatter spectrum (Fig. 29C). A white-gray volcanic ash layer at 29 mbsf of Hole 1011C displayed reflectance values near 25%, greater than the ~10% values for ash layers at Site 1010 (Fig. 29D). The spectra are also different, with the Site 1011 ash showing reflectance minima in the infrared and ultraviolet ranges and a maximum near 650 nm.

Color reflectance data from Hole 1011B were used to predict sedimentary opal content in real time aboard ship. Using a regression

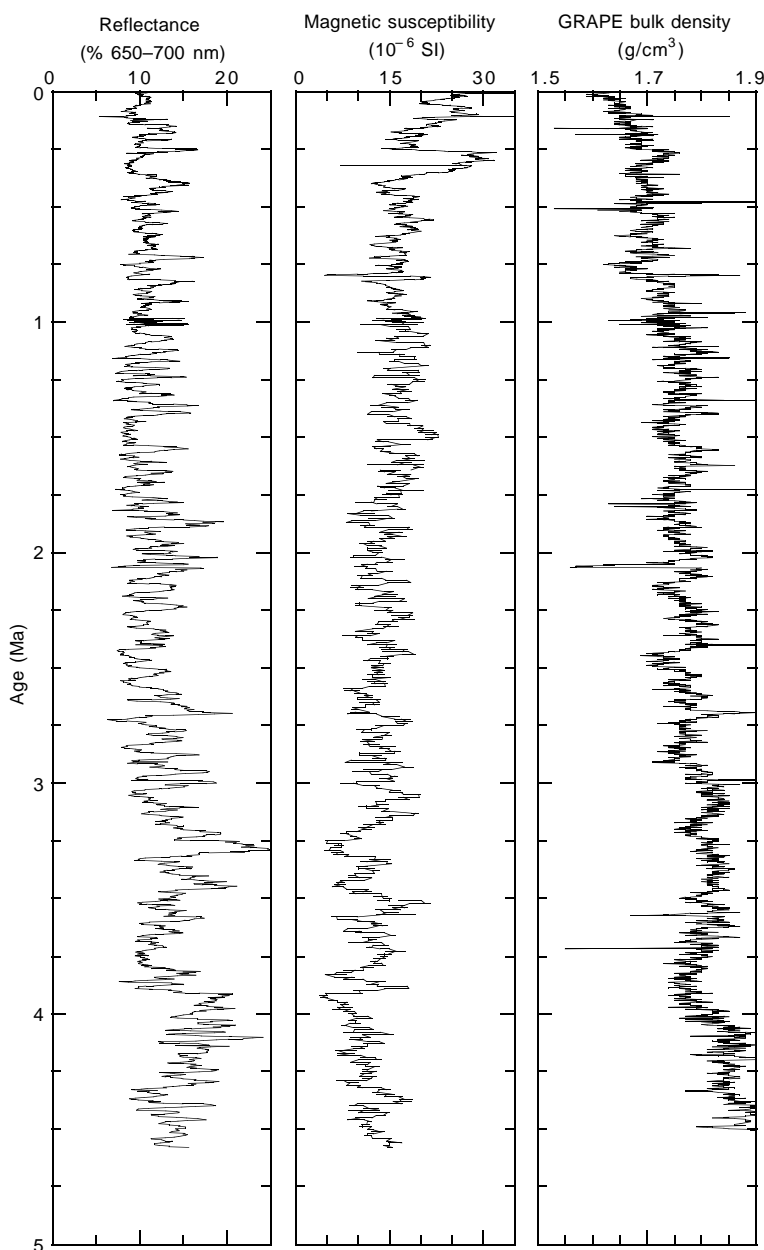


Figure 16. Spliced records of color reflectance, magnetic susceptibility, and GRAPE bulk density vs. age based on age control points from Table 12.

equation generated from the Leg 167 site-survey reflectance and opal data, we were able to simulate the major lithostratigraphic units identified at Site 1011. Low opal content coincides with lithostratigraphic Units I and II, which include silty clay and nannofossil ooze and chalk (Fig. 30A). Peaks and lows in opal in lithostratigraphic Unit III correspond to interbedded diatomite and clay, respectively. Opal levels are low in the siltstone, silty clay, and sandstone of lithostratigraphic Unit IV. The highest predicted opal content at Site 1011 (from 245 to 255 mbsf) matches the portion of lithostratigraphic Unit III classified as a diatomite (Fig. 30B). Preliminary results indicate that opal-rich sediments display a unique reflectance spectrum, with an absorbance peak near 650 nm and a steep positive slope in the red to infrared range (Fig. 30C). In contrast, sediments with low predicted opal content display a much flatter spectrum (Fig. 30D). Figure 30 is qualitatively similar in shape, although not in absolute brightness, to the reflectance spectra of siliceous sediments at Leg 138 sites in the eastern equatorial Pacific (Mayer, Pisias, Janecek, et al., 1992).

Digital Color Video

Images from the ODP color digital imaging system at Holes 1011B, 1011C, and 1011E were taken over 20-cm intervals to provide a 0.25-mm pixel. The intensity of colors CIELAB L^* , a^* , and b^* (“Explanatory Notes” chapter, this volume) shows a good correlation between Holes 1011B and 1011C (Fig. 31).

DOWNHOLE MEASUREMENTS Logging Operations and Log Quality

Hole 1011B was logged with the density-porosity combination and sonic-FMS tool strings after the hole was flushed of debris and the drill pipe was set at 77 mbsf (Table 19). Two full passes of the density-porosity combination tool string (pass 1: 80–277 mbsf; pass 2: 96–278 mbsf) and one full pass of the sonic-FMS tool string (99–

Table 13. Interstitial water geochemical data, Hole 1011B.

Core, section, interval (cm)	Depth (mbsf)	pH	Alkalinity (mM)	Salinity	Cl ⁻ (mM)	Na ⁺ (mM)	SO ₄ ²⁻ (mM)	HPO ₄ ²⁻ (μM)	NH ₄ ⁺ (μM)	H ₄ SiO ₄ (μM)	Mn ²⁺ (μM)	Ca ²⁺ (mM)	Mg ²⁺ (mM)	Sr ²⁺ (μM)	Li ⁺ (μM)	K ⁺ (mM)
167-1011B-																
1H-3, 140–145	4.45	7.64	8.28	35.0	549	475	23.2	37	472	494	16.5	8.87	50.0	80	27	11.3
2H-3, 145–150	12.85	7.70	14.0	34.0	561	486	14.9	41	1148	500	7.0	6.14	47.3	88	33	11.8
3H-3, 145–150	22.35	7.72	17.7	34.0	563	488	8.0	49	1664	646	5.5	4.67	43.9	103	36	12.1
4H-3, 145–150	31.85	7.72	19.5	32.5	560	485	4.2	49	1933	678	<5	3.96	41.0	121	39	13.1
5H-3, 145–150	41.35	7.72	20.1	32.0	561	486	<1	45	2209	791	<5	3.36	38.4	144	43	11.2
6H-3, 145–150	50.85	7.64	21.6	32.0	559	485	<1	47	2471	823	<5	4.16	37.7	174	51	11.7
9H-3, 145–150	79.35	7.36	22.6	32.0	559	488	<1	30	2842	840	<5	5.93	35.7	191	74	10.6
12H-3, 145–150	107.85	7.30	19.2	32.0	556	485	<1	20	2587	1028	<5	6.61	33.6	174	98	9.5
15H-3, 145–150	136.35	7.26	14.9	32.0	558	486	<1	11	2616	918	<5	7.18	31.6	155	10	9.8
18X-3, 145–150	160.65	7.34	11.3	32.0	560	488	6.6	6	2195	1103	<5	9.15	34.8	144	99	8.7
21X-3, 145–150	189.45	7.24	8.62	33.0	556	487	16.1	5	1890	1216	<5	12.0	38.7	128	73	8.7
24X-3, 145–150	218.35	7.49	6.95	34.0	557	480	19.5	3	1345	1367	<5	14.8	42.9	113	54	8.1
27X-3, 145–150	247.25	7.41	5.05	34.5	559	478	23.5	2	974	1457	<5	16.5	44.9	105	39	9.9

282 mbsf) were conducted. The wireline heave compensator was used on all passes although seas were calm.

Borehole caliper measurements conducted during the density-porosity combination and sonic-FMS passes indicate that the borehole was nearly at drill-bit diameter (12–13 in.; Fig. 32) with few wash-outs. Overall log quality at this site was very good with the exception of the sonic velocity log, which was unable to measure formation velocities because of the unusually high porosity of the sediments and consequent low-impedance contrast with respect to the borehole fluid (seawater). Shipboard processing of the sonic waveform data to extract formation compressional wave velocities was also unsuccessful. Sonic velocity data from this hole are therefore considered unreliable.

The TLT was run during both passes of the density-porosity combination tool string. The temperature logs were linked to the actual logging depths using the time-depth log recorded at the logging unit. The TLT results show a downhole thermal gradient of 31°C/km (Fig. 33), although this is an underestimate resulting from the cooling effect of open-hole circulation during drilling. In situ temperature measurements using the Adara probe indicate a thermal gradient near 108°C/km at this site (see “Physical Properties” section, this chapter).

Lithology

The lithologic succession recovered at Hole 1011B is characterized by large shifts in sediment composition and compaction that are reflected clearly in the log physical property measurements. In particular, the increased lithification and reduced carbonate content associated with the lithostratigraphic Subunit IIA/Subunit IIB boundary near 130 mbsf (Fig. 32) is identified in the log data as a sharp increase in bulk density and resistivity and a reduction in porosity. Similarly, the sharply increased diatom content of lithostratigraphic Subunit IIIA is reflected by a reduction of density and resistivity and an increased porosity below 200 mbsf. Although the velocity log measurements are not reliable at this site, these two lithologic boundaries must have strong seismic impedance signatures. Fine-scale (~1 m) interbedding is apparent in the SFL data and the processed FMS imagery in the portions of lithostratigraphic Subunit IIIA with a higher sedimentation rate (200–260 mbsf).

Comparison of Core and Log Physical Property Data

The core and log measurements of sediment bulk density are similar over their common interval, whereas the core porosity data (see “Physical Properties” section, this chapter) are significantly lower than the log (neutron) measurements (Fig. 34). The log porosity (neutron) data are significantly higher because the data reflect the influence of molecularly bound water associated with abundant clay and opal in Hole 1011B sediments, which contribute additional apparent porosity in the log porosity measurement. Density measurements of the litho-density logging tool (HLDT) can be used to estimate sedi-

ment porosity as well, using the assumption that pore spaces are water filled. Because this tool uses a different method for investigating formation density (gamma-ray emission from a ¹³⁷Cs source), it provides an alternative method to evaluate porosity. The log neutron porosity and litho-density porosity measurements are compared with the core porosity data in Figure 35. Note the closer match between the log litho-density porosity measurements and core porosity data.

Comparison of Core and Log Data

Core MST measurements and log measurements of natural gamma ray and bulk density shown in Figure 36 exhibit comparable large-scale variability, although fine-scale (<1 m) correlation between the core and log data sets is difficult because of the fine-scale nature of the bedding cycles, lower vertical resolution of the log data, and core disturbance resulting from gas expansion. Gas expansion and XCB coring disturbance particularly affected the volume-dependent MST core measurements of bulk density and natural gamma ray activity. The switch from APC to XCB coring (~138 mbsf) and the consequent development of sediment slurry in core liners are apparent as a sharp decrease in the GRAPE measurement of sediment bulk density (Fig. 36).

A more detailed comparison of core and log measurements of natural gamma-ray activity and bulk density is shown in Figure 37 for the 180–200 mbsf interval in Hole 1011B, spanning the lithostratigraphic Subunit IIC/Subunit IIIA boundary. The core and log data show similar large-scale variability, but finer scale correlation is more difficult to establish. Significantly, the log data appear highly repeatable both in absolute depth and value between the two separate passes.

SUMMARY

Site 1011, in the Animal Basin of the California Borderland, is the shoreward site of the Baja Transect located 85 km west of Baja California. Although the water depth at this site is 2033 mbsl, the basin sill depth is ~1600 mbsl. The bottom waters within Animal Basin are relatively pristine intermediate waters from offshore that have traveled only a short distance from the open ocean. We achieved our objective to drill the entire 276-m-thick sediment column to acoustic basement, which turned out to be basalt (Fig. 38). Oldest sediments are upper Miocene sandstones with an age of ~9.3 Ma. The sediment column was triple cored to 142 mbsf (~4.4 Ma), and double cored to 184 mbsf (~6.7 Ma). A continuous section could only be verified for the triple-cored section. Paleomagnetic measurements are poor at Site 1011, and the only time control is provided by biostratigraphy. Distinctive features to note within the lithostratigraphic column are the basalt basement, which may reflect volcanism associated with the formation of the borderland basins, the terrigenous clastic basal unit

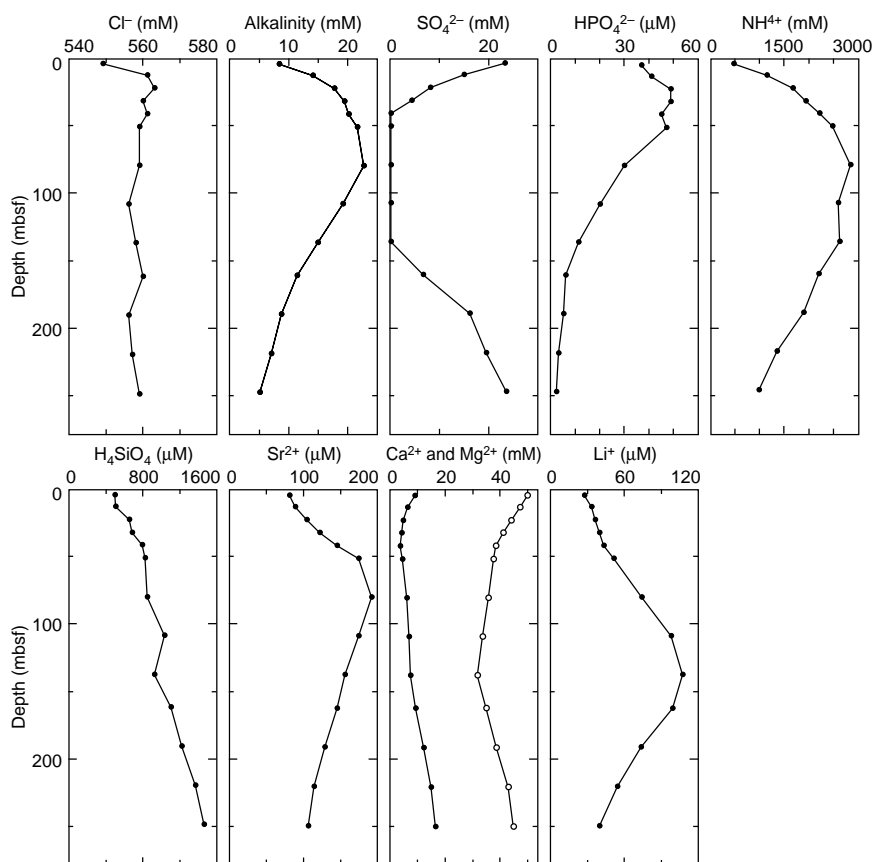


Figure 17. Interstitial water geochemical data, Site 1011. Solid circles = Ca, open circles = Mg.

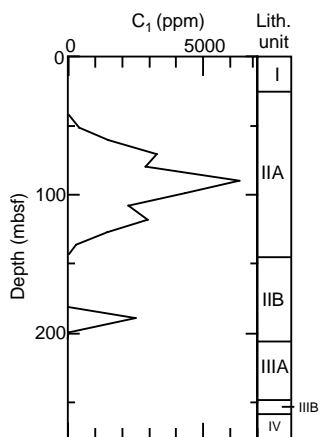


Figure 18. Concentration of methane (C_1) vs. depth (mbsf) obtained by the headspace technique from Holes 1011A and 1011B.

older than 8.5 Ma, the abrupt change from diatomaceous to calcareous sediments at about 7.5 Ma (~2 m.y. older than at Site 1010), and the abrupt drop in calcium carbonate burial younger than the Miocene/Pliocene boundary (~4.6 Ma, lithostratigraphic Unit IIB/Unit IIC transition). The Unit IIB/Unit IIC transition appears seismically as the boundary between the acoustically transparent sediments above and the more distinctively layered sediments below (Fig. 38). High calcium carbonate content returns between 3.8 and 1.0 Ma, but

Table 14. Concentrations of methane (C_1) and ethane/ethylene (C_2) obtained by the headspace technique from Holes 1011A and 1011B.

Core, section, interval (cm)	Depth (mbsf)	C_1 (ppm)	C_2 (ppm)	C_1/C_2
167-1011A-1H-4, 0-5	6.425	3		
167-1011B-1H-4, 0-5	4.525	4		
2H-4, 0-5	12.925	6		
3H-4, 0-5	22.425	5		
4H-4, 0-5	31.925	11		
5H-4, 0-5	41.425	49		
6H-4, 0-5	50.925	424		
7H-4, 0-5	60.425	1505		
8H-4, 0-5	69.925	3269		
9H-4, 0-5	79.425	2857		
10H-4, 0-5	88.925	6347		
11H-4, 0-5	98.425	4334		
12H-4, 0-5	107.93	2226		
13H-4, 0-5	117.43	2954		
14H-4, 0-5	126.93	1452		
15H-4, 0-5	136.43	298		
16X-4, 0-5	142.43	27		
17X-4, 0-5	151.03	11		
18X-4, 0-5	160.73	6		
19X-4, 0-5	170.23	7		
20X-4, 0-5	179.93	4		
21X-4, 0-5	189.53	2505	6	439
22X-4, 0-5	199.13	88		
23X-4, 0-5	208.83	8		
24X-4, 0-5	218.43	6	1	6
25X-4, 0-5	228.03	7		
26X-4, 0-5	237.73	7		
27X-4, 0-5	247.33	6		
28X-4, 0-5	256.93	5		

Table 15. Depth variations in concentration of inorganic carbon, calcium carbonate, total carbon, total organic carbon, total nitrogen, and total sulfur in weight percent (wt%) in Hole 1011B.

Core, section, interval (cm)	Depth (mbsf)	Inorganic carbon (wt%)	CaCO ₃ (wt%)	Total carbon (wt%)	Total organic carbon (wt%)	Total nitrogen (wt%)	Total sulfur (wt%)	Total organic carbon/total nitrogen	Total organic carbon/total sulfur
167-1011B-									
1H-1, 29-30	0.29	2.00	16.7	3.54	1.54	0.18	0.37	8.6	4.2
1H-2, 29-30	1.79	0.71	5.9	2.19	1.48	0.17	0.46	8.7	3.2
1H-3, 29-30	3.34	0.77	6.4	2.26	1.49	0.17	0.38	8.8	3.9
1H-4, 29-30	4.79	0.13	1.1	2.38	2.25	0.25	0.59	9.0	3.8
1H-5, 29-30	6.29	0.55	4.6	1.81	1.26	0.16	0.31	7.9	4.1
1H-6, 29-30	7.79	2.11	17.6	3.10	0.99	0.11	1.53	9.0	0.6
2H-2, 30-31	10.20	0.18	1.5	1.82	1.64	0.18	0.40	9.1	4.1
2H-3, 30-31	11.70	1.40	11.7	2.31	0.91	0.10	0.17	9.1	5.4
2H-4, 30-31	13.20	0.37	3.1	1.83	1.46	0.17	0.53	8.6	2.8
2H-5, 30-31	14.70	1.00	8.3	1.95	0.95	0.11	0.18	8.6	5.3

Only part of this table is produced here. The entire table is on CD-ROM, back pocket, this volume.

the subsequent upper Pleistocene sediment is very clay-rich and microfossil-poor.

REFERENCES

- Akiba, F., 1986. Middle Miocene to Quaternary diatom biostratigraphy in the Nankai trough and Japan trench, and modified lower Miocene through Quaternary diatom zones for middle-to-high latitudes of the North Pacific. In Kagami, H., Karig, D.E., Coulbourn, W.T., et al., *Init. Repts. DSDP, 87*: Washington (U.S. Govt. Printing Office), 393-481.
- Barron, J.A., 1992. Neogene diatom datum levels in the equatorial and North Pacific. In Ishizaki, K., and Saito, T. (Eds.), *The Centenary of Japanese Micropaleontology*: Tokyo (Terra Sci. Publ.), 413-425.
- Bordovskiy, O.K., 1965. Accumulation and transformation of organic substances in marine sediment, 2. Sources of organic matter in marine basins. *Mar. Geol.*, 3:5-31.
- Canfield, D.E., and Berner, R.A., 1987. Dissolution and pyritization of magnetite in anoxic marine sediments. *Geochim. Cosmochim. Acta*, 51:645-659.
- Emerson, S., and Hedges, J.I., 1988. Processes controlling the organic carbon content of open ocean sediments. *Paleoceanography*, 3:621-634.
- Ingle, J.C., Jr., 1981. Origin of Neogene diatomites around the north Pacific rim. In Garrison, R.E., Douglas, R., Pisciotto, K., Isaacs, C., and Ingle, J.C. (Eds.), *The Monterey Formation and Related Siliceous Rocks of California*. Spec. Publ.—Soc. Econ. Paleontol. Mineral., 15:159-179.
- Karlin, R., and Levi, S., 1983. Diagenesis of magnetic minerals in recent hemipelagic sediments. *Nature*, 303:327-330.
- Koizumi, I., and Tanimura, Y., 1985. Neogene diatom biostratigraphy of the middle latitude western North Pacific, Deep Sea Drilling Project Leg 86. In Heath, G.R., Burckle, L.H., et al., *Init. Repts. DSDP, 86*: Washington (U.S. Govt. Printing Office), 269-300.
- Leslie, B.W., Lund S.P., and Hammond, D.E., 1990. Rock magnetic evidence for the dissolution and authigenic growth of magnetic minerals within anoxic marine sediments of the California continental borderland. *J. Geophys. Res.*, 95:4437-4452.
- Lonsdale, P., 1991. Structural patterns of the Pacific floor offshore of Peninsular California. In Dauphin, J.P., and Simoneit, B.R.T. (Eds.), *The Gulf and Peninsular Province of the Californias. Amer. Assoc. Petrol. Geol. Memoir 47*, 87-125.
- Lund, S.P., Gorsline, D.S., and Henyey, T.L., 1992. Rock magnetic characteristics of surficial marine sediments from the California Continental Borderland. *Earth Planet. Sci. Lett.*, 108:93-107.
- Lyle, M., Gallaway, P.J., Liberty, L.M., Mix, A., Stott, L., Hammond, D., Gardner, J., Dean, W., and the EW9504 Scientific Party, 1995a. Data submission: W9406 and EW9504 site surveys of the California margin proposed drillsites, Leg 167. Volume 1: Site maps and descriptions. Boise State Univ., *CGISS Tech. Rept.*, 95-11.
- Lyle, M., Gallaway, P.J., Liberty, L.M., Mix, A., Stott, L., Hammond, D., Gardner, J., Dean, W., and the EW9504 Scientific Party, 1995b. Data submission: W9406 and EW9504 site surveys of the California margin proposed drillsites, Leg 167. Volume 2: Seismic profiles. Boise State Univ., *CGISS Tech. Rept.*, 95-12.
- Mayer, L., Pisias, N., Janecek, T., et al., 1992. *Proc. ODP, Init. Repts.*, 138 (Pts. 1 and 2): College Station, TX (Ocean Drilling Program).
- McCrorry, P.A., Wilson, D.S., Ingle, J.C., Jr., and Stanley, R.G., 1995. Neogene geohistory analysis of Santa Maria Basin, California and its relationship to transfer of central California to the Pacific Plate. In Keller, M.A. (Ed.), *Evolution of Sedimentary Basins/Onshore Oil and Gas Investigations—Santa Maria Province*. U.S. Geol. Surv. Bull., J:1-38.
- Okada, H., and Bukry, D., 1980. Supplementary modification and introduction of code numbers to the low-latitude coccolith biostratigraphic zonation (Bukry, 1973; 1975). *Mar. Micropaleontol.*, 5:321-325.
- Zellers, S.D., 1995. Foraminiferal biofacies, paleoenvironments, and biostratigraphy of Neogene-Quaternary sediments, Cascadia Margin. In Carson, B., Westbrook, G.K., Musgrave, R.J., and Suess, E. (Eds.), *Proc. ODP, Sci. Results*, 146 (Pt. 1): College Station, TX (Ocean Drilling Program), 79-113.

Ms 1671R-105

NOTE: For all sites drilled, core-description forms (“barrel sheets”) and core photographs can be found in Section 3, beginning on page 499. Smear-slide data can be found in Section 4, beginning on page 1327. Thin section data can be found in Section 5, beginning on page 1375. See Table of Contents for material contained on CD-ROM.

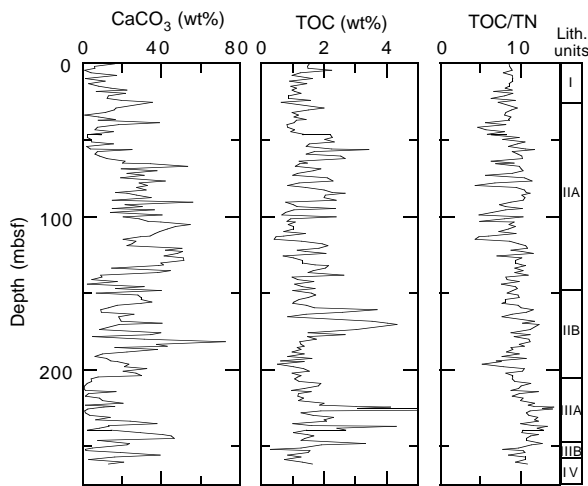


Figure 19. Calcium carbonate and total organic carbon data in weight percent (wt%) and TOC/TN vs. depth (mbsf) from sediments of Hole 1011B.

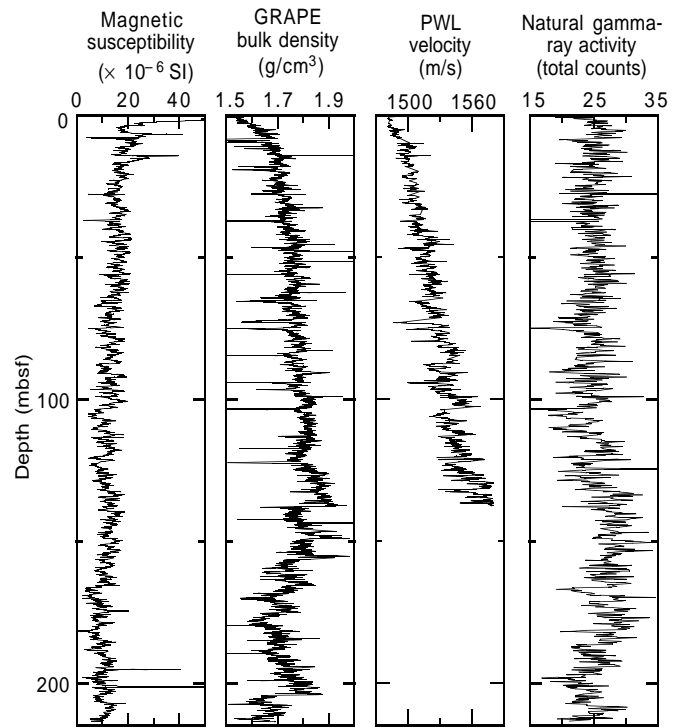


Figure 22. MST data from Hole 1011B.

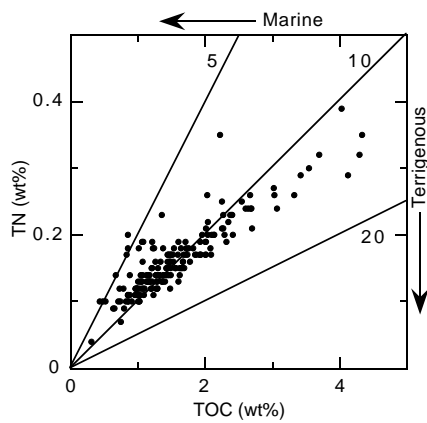


Figure 20. Total nitrogen (TN) vs. total organic carbon (TOC) from sediments of Hole 1011B. TOC/TN values below 10 suggest a predominance of marine organic matter. TOC/TN values above 10 suggest a predominance of terrigenous organic matter.

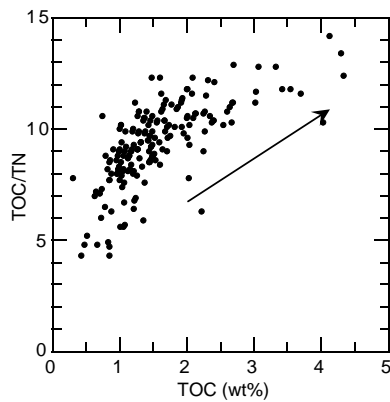


Figure 21. Total organic carbon (TOC) vs. total organic carbon/total nitrogen values (TOC/TN) in sediments of Hole 1011B. Arrow indicates correlation of higher TOC values with increased TOC/TN ratios.

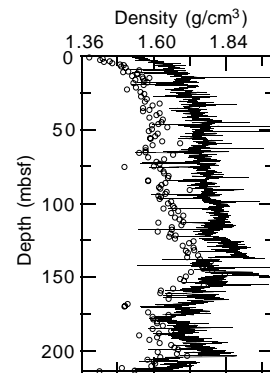


Figure 23. GRAPE bulk density (line) and index property bulk density (circles) data from Hole 1011B.

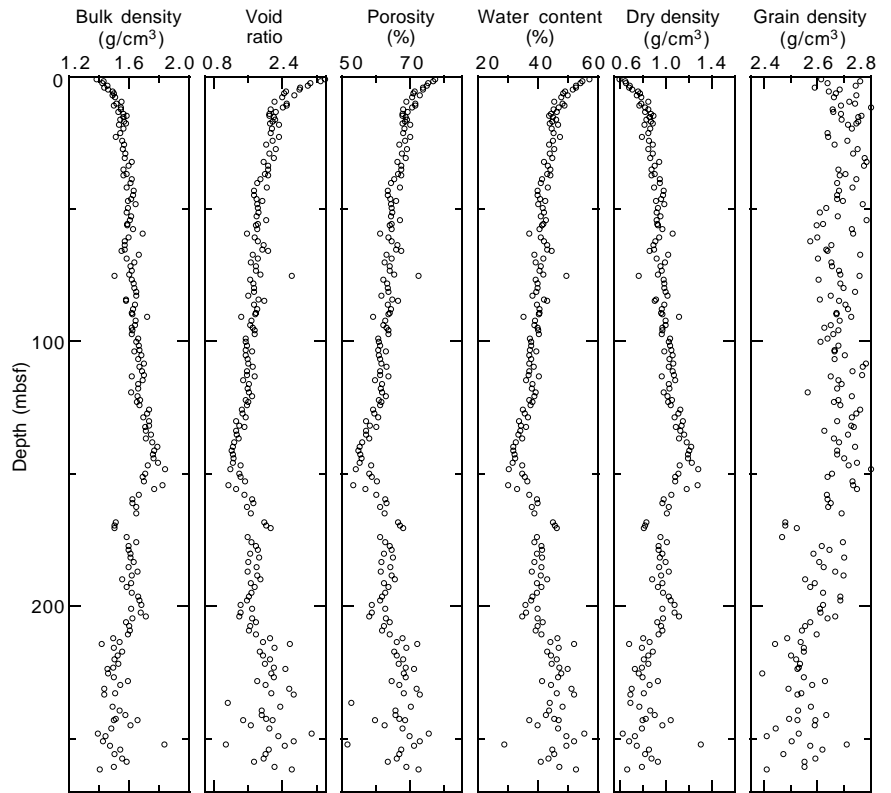


Figure 24. Index properties data from Hole 1011B.

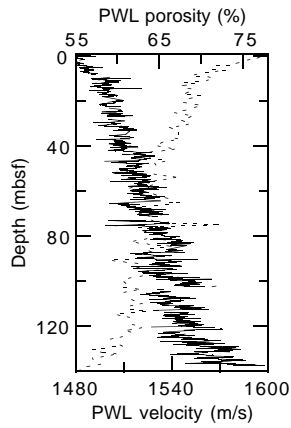


Figure 25. PWL velocity (line) and index property porosity (dashed line) data from Hole 1011B.

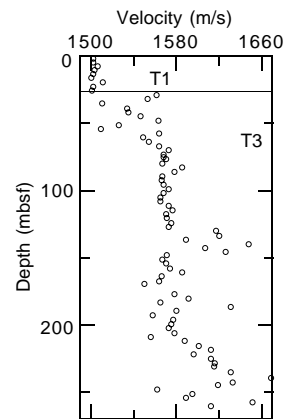


Figure 26. Discrete velocity values from Hole 1011B determined using two different transducer pairs. Pair T1 was used above 26 mbsf (solid horizontal line) and pair T3 was used at greater depths.

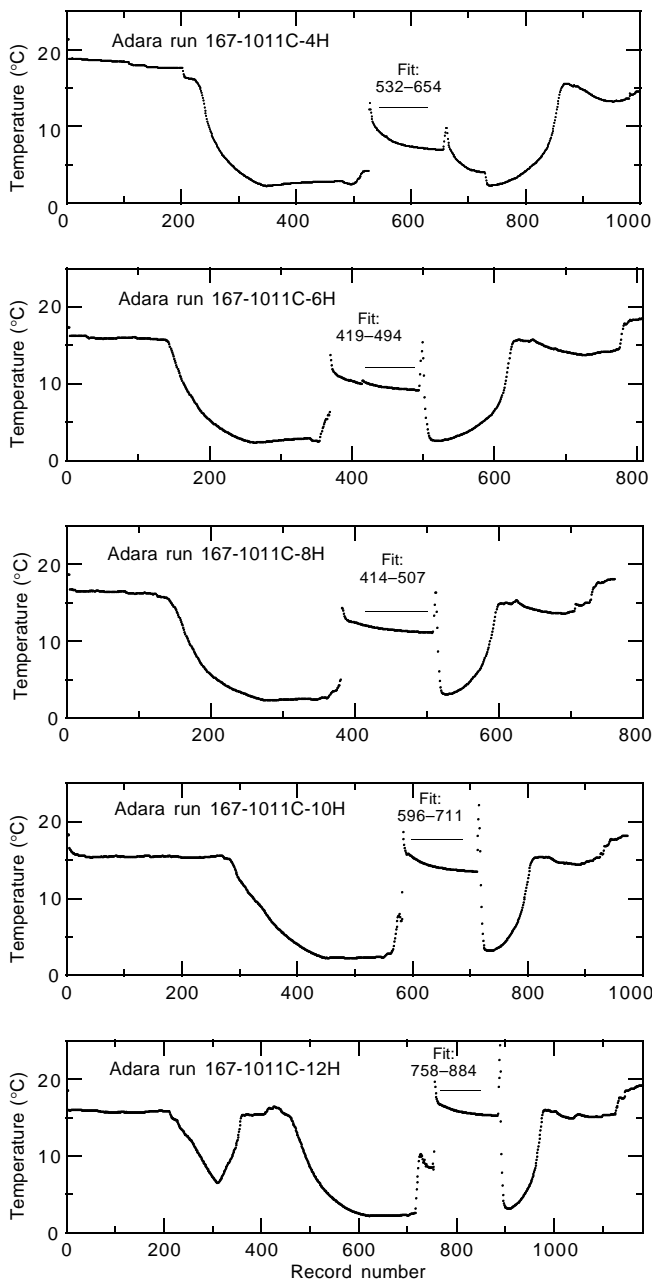


Figure 27. Hole 1011C downhole temperature vs. record number (5-s recording frequency) for each measurement run, showing the interval fitted to determine the downhole temperature.

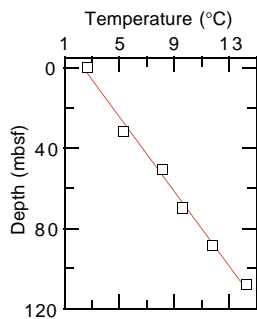


Figure 28. Downhole temperature gradient for Hole 1011C.

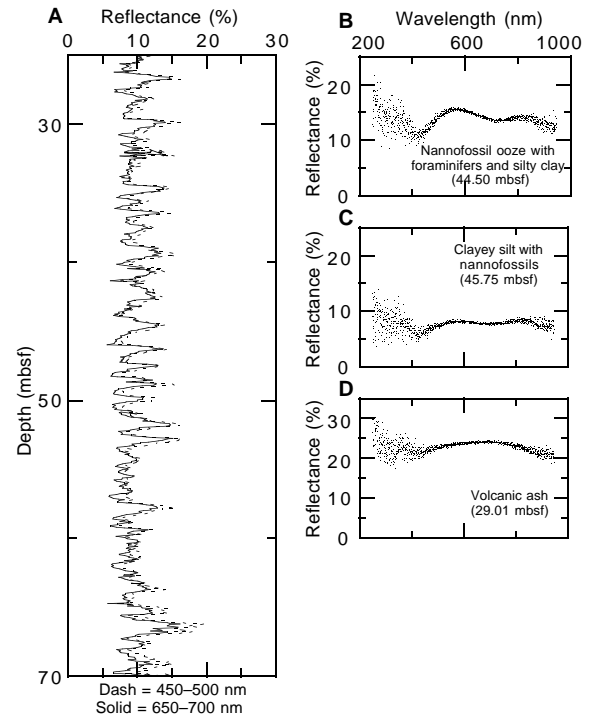


Figure 29. Summary of color reflectance data for Hole 1011C. **A.** Percent reflectance of two band averages (450–500 and 650–700 nm) from 25 to 70 mbsf. **B.** Characteristic spectra of nannofossil ooze with silty clay. **C.** Spectra of a clayey silt with nannofossils. **D.** High-reflectance ash layer.

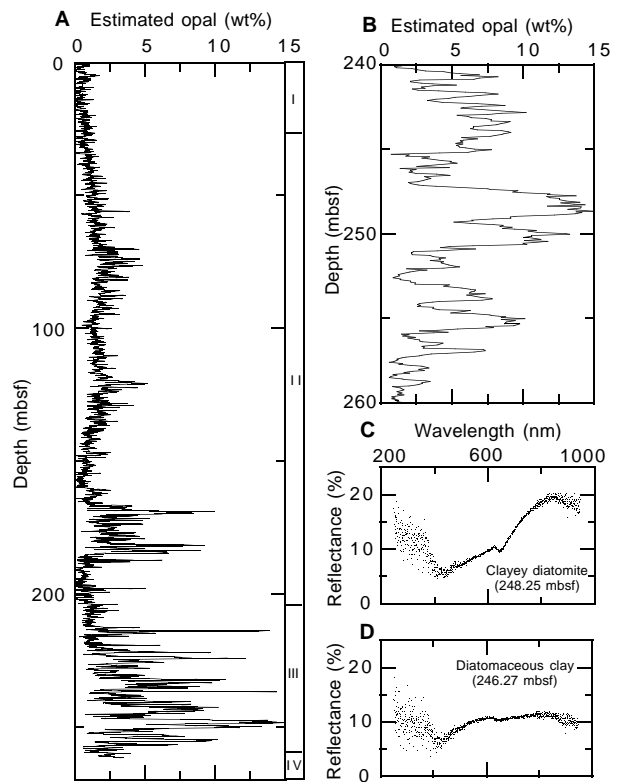


Figure 30. Summary of weight-percent opal prediction for Hole 1011C. **A.** Complete downhole opal prediction and corresponding major lithostratigraphic units. **B.** Close-up of opal prediction for 240–260 mbsf. **C.** Characteristic spectra of a clayey diatomite at the 248.25-mbsf opal peak. **D.** Relatively flat spectra from opal low at 246.27 mbsf.

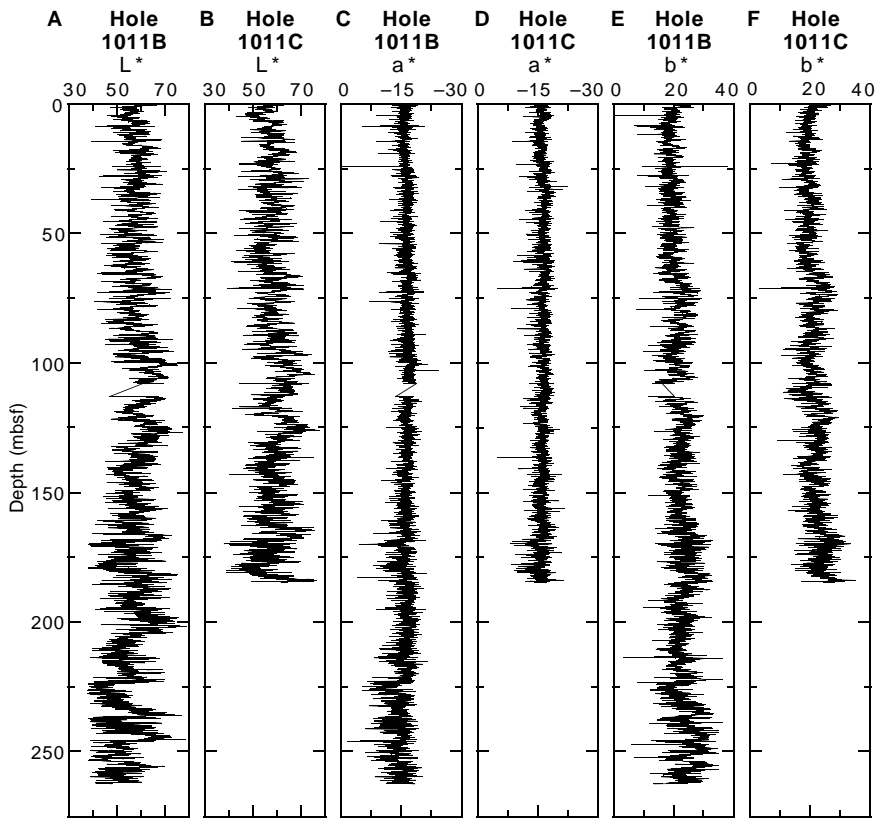


Figure 31. Digital color video data from Holes 1011B and 1011C. **A.** Intensity of color CIELAB L* from Hole 1011B. **B.** Intensity of color CIELAB L* from Hole 1011C. **C.** Intensity of color CIELAB a* from Hole 1011B. **D.** Intensity of color CIELAB a* from Hole 1011C. **E.** Intensity of color CIELAB b* from Hole 1011B. **F.** Intensity of color CIELAB b* from Hole 1011C. CIELAB data decimated to 2-cm intervals.

Table 19. Downhole measurements at Hole 1011B.

Date, time	Description
1 May 1996	
0700	Set pipe at 77 mbsf, start wireline rig up, seas calm.
0815	Finish wireline rig up, RIH density-porosity combination tool string.
0950	At TD (277.5 mbsf), wireline heave compensator on, start density-porosity pass 1 (277–80 mbsf); 300 m/hr.
1110	At TD (277.5 mbsf), wireline heave compensator on, start density-porosity pass 2 (278–96 mbsf), 300 m/hr continue log recording to mudline.
1400	Rig down density-porosity combination tool string, rig up and RIH with sonic-FMS tool string.
1500	At TD, wireline heave compensator on, begin sonic-FMS pass 1 (282–99 mbsf).
1600	End sonic-FMS pass 1. FMS calipers not closing, circulate with mudpumps.
1715	POOH sonic-FMS, rig down.

Note: RIH = run in hole, TD = total depth, FMS = Formation MicroScanner, POOH = pull out of hole.

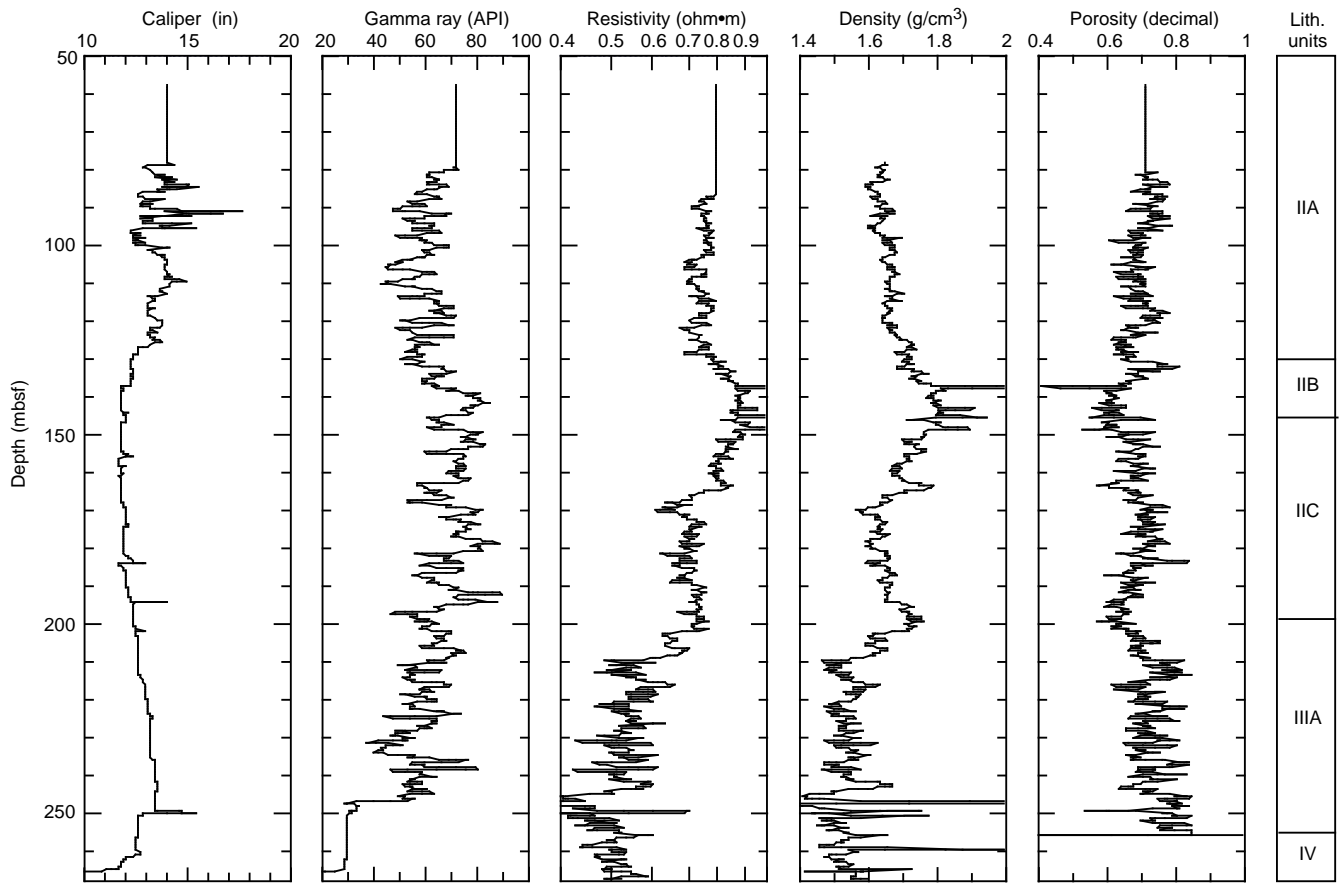


Figure 32. Downhole log data from the density-porosity combination tool string (pass 1) and a lithostratigraphic summary column at Hole 1011B (see “Lithostratigraphy” section, this chapter).

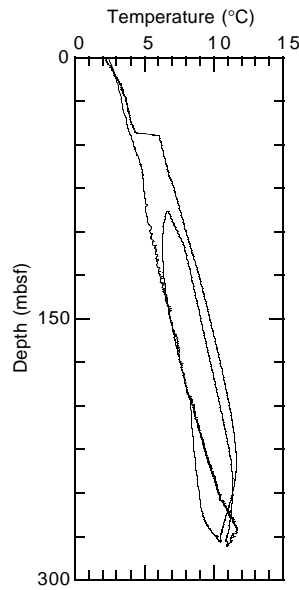


Figure 33. Borehole temperature measurements from the Lamont-Doherty temperature logging tool.

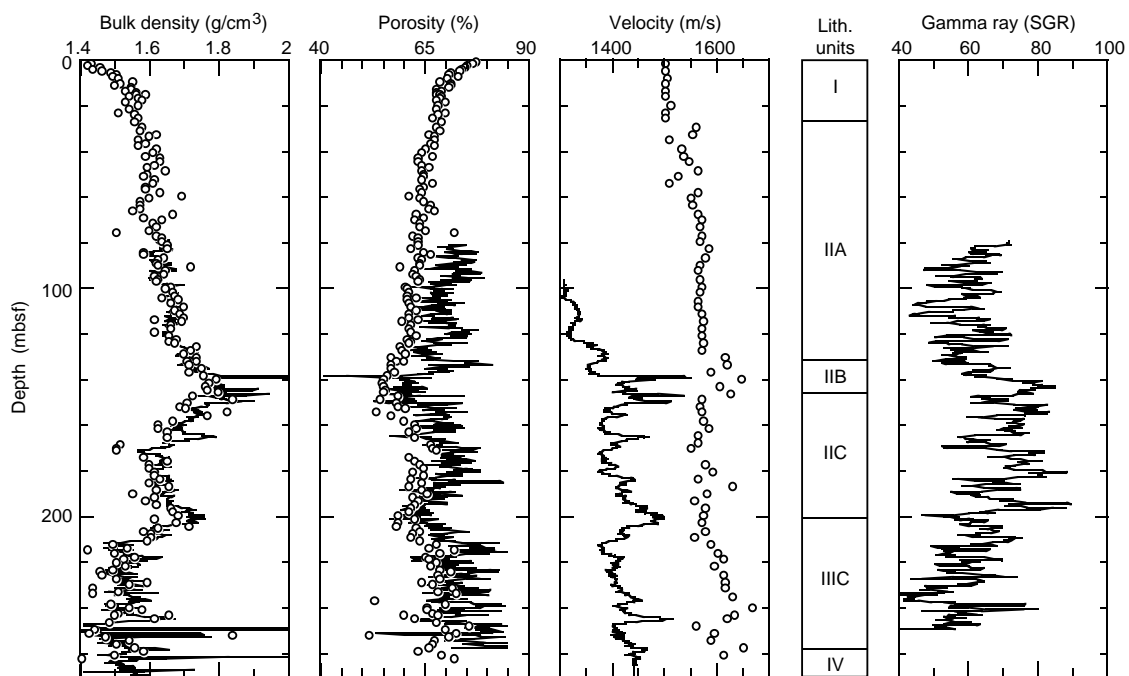


Figure 34. Comparison of core (open symbols) and log (line) physical property data.

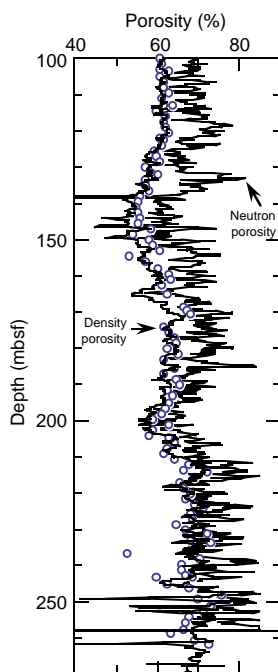


Figure 35. Neutron and litho-density log measurements of formation porosity (lines) compared to core porosity (open symbols) measurements.

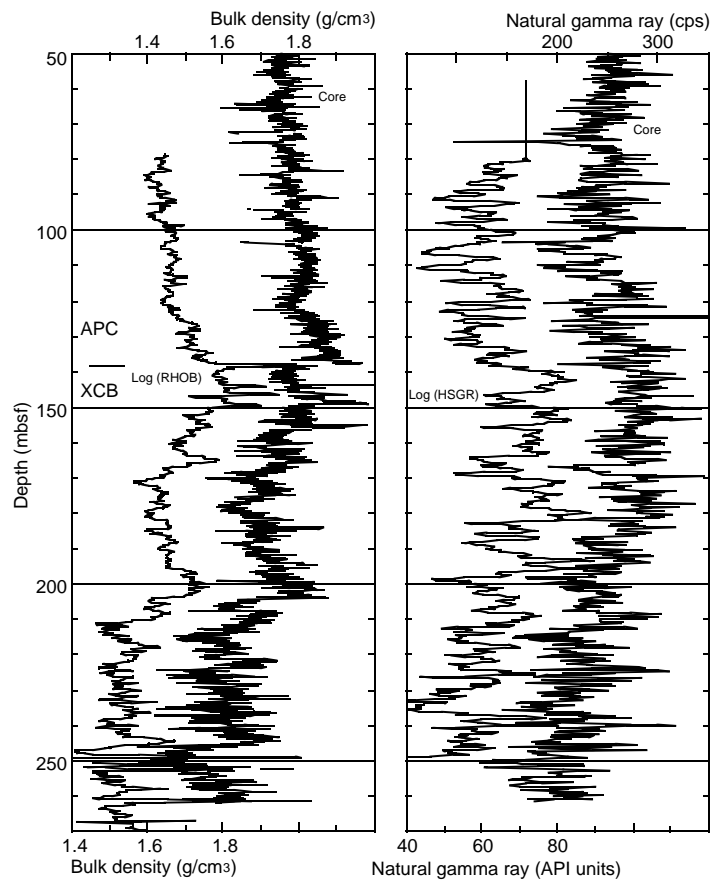


Figure 36. Comparison of core (MST) with log natural gamma-ray and bulk density data at Hole 1011B. Note the reduced core bulk densities associated with the switch from APC to XCB coring at ~138 mbsf.

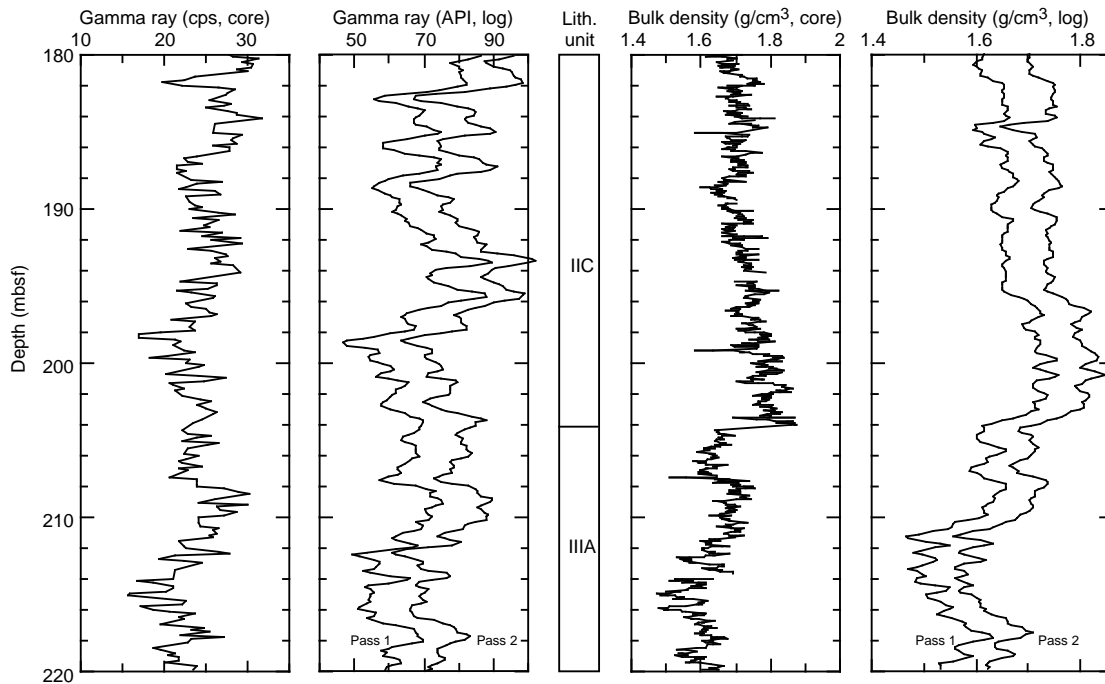


Figure 37. Detail of the core and log natural gamma-ray and bulk density data at Hole 1011B, 180–220 mbsf. Log data from passes 1 and 2 are shown to illustrate log repeatability.

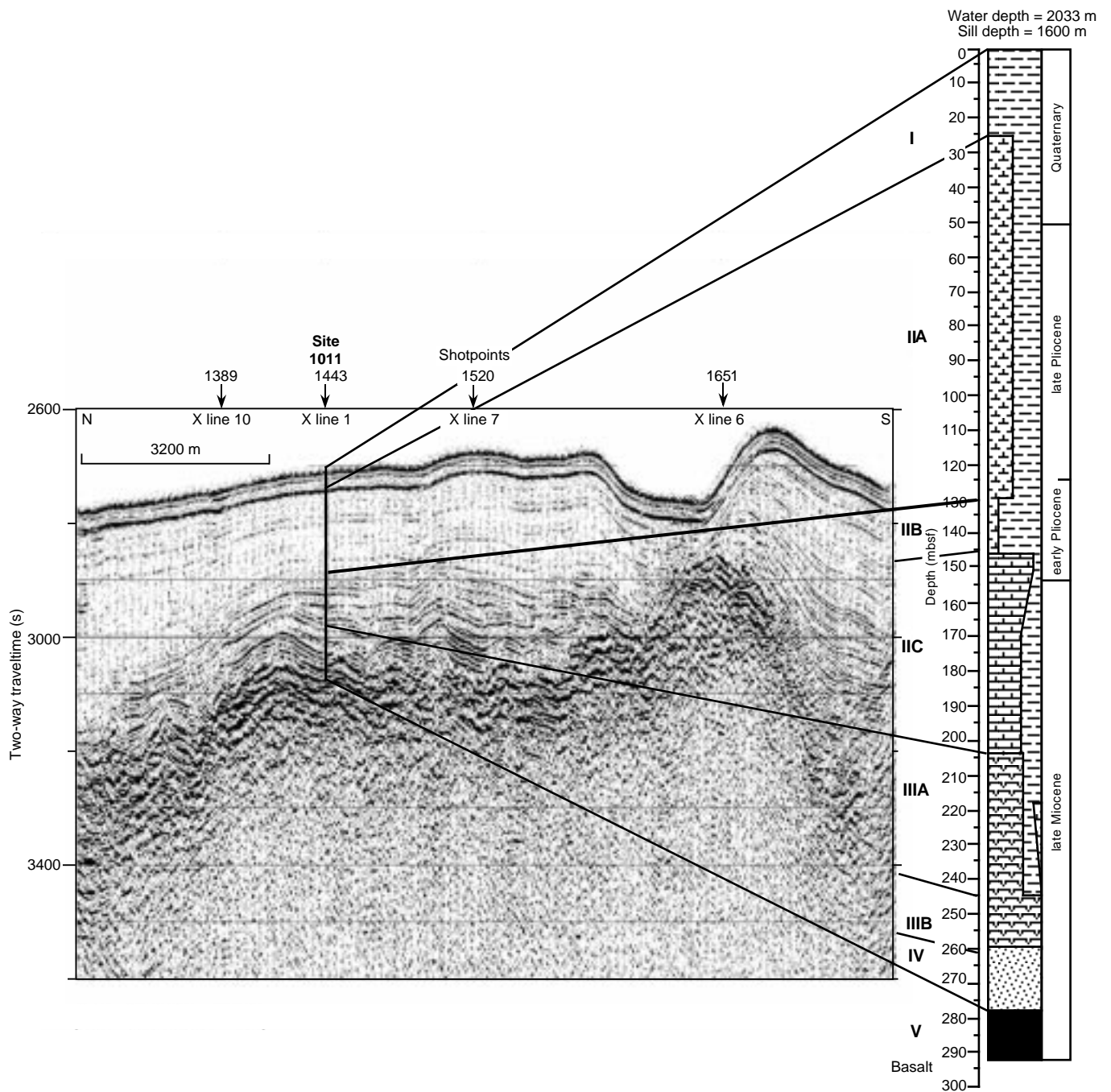


Figure 38. Comparison of the lithostratigraphic column at Site 1011 and a seismic profile through the site (Line EW9504 CAM2-2; Lyle et al., 1995b). Ties are estimated from the depth to basement and measured seismic velocities (see "Physical Properties" section, this chapter). On y-axis, (s) = milliseconds.

SHORE-BASED LOG PROCESSING Hole 1011B

Bottom felt: 2032.5 mbrf (used for depth shift to seafloor)

Total penetration: 281.5 mbsf

Total core recovered: 271.1 m (96%)

Logging Runs

Logging string 1: DIT/HLDT/APS/HNGS (2 passes)

Logging string 2: FMS/GPIT/SDT/NGT

Wireline heave compensator was used to counter ship heave.

Bottom-Hole Assembly

The following bottom-hole assembly depths are as they appear on the logs after differential depth shift (see "Depth shift" section) and depth shift to the sea floor. As such, there might be a discrepancy with the original depths given by the drillers on board. Possible reasons for depth discrepancies are ship heave, use of wireline heave compensator, and drill string and/or wireline stretch.

DIT/HLDT/APS/HNGS: Did not reach bottom-hole assembly.

DIT/HLDT/APS/HNGS: Bottom-hole assembly at ~49.5 mbsf (pass 2).

FMS/GPIT/SDT/NGT: Did not reach bottom-hole assembly.

Processing

Depth shift: Original logs have been interactively depth shifted with reference to NGT from DIT/SDT/HLDT/APS/HNGS pass 2 and to the seafloor (-2032.5 m).

Gamma-ray and environmental corrections: Corrections for borehole size and type of drilling fluid were performed on the NGT data from the FMS/GPIT/SDT/NGT tool string. HNGS data from the DIT/HLDT/APS/HNGS tool string were corrected in real-time during the recording.

Acoustic data processing: The array sonic tool was operated in standard depth-derived, borehole compensated, long spacing (8-10-10-12 ft) and short spacing (3-5-5-7 ft) mode. The sonic logs from the long spacing mode have been processed to eliminate some of the noise and cycle skipping experienced during the recording.

Quality Control

Data recorded through bottom-hole assembly, such as the HNGS data above 50 mbsf (pass 1) should be used qualitatively only because of the attenuation on the incoming signal.

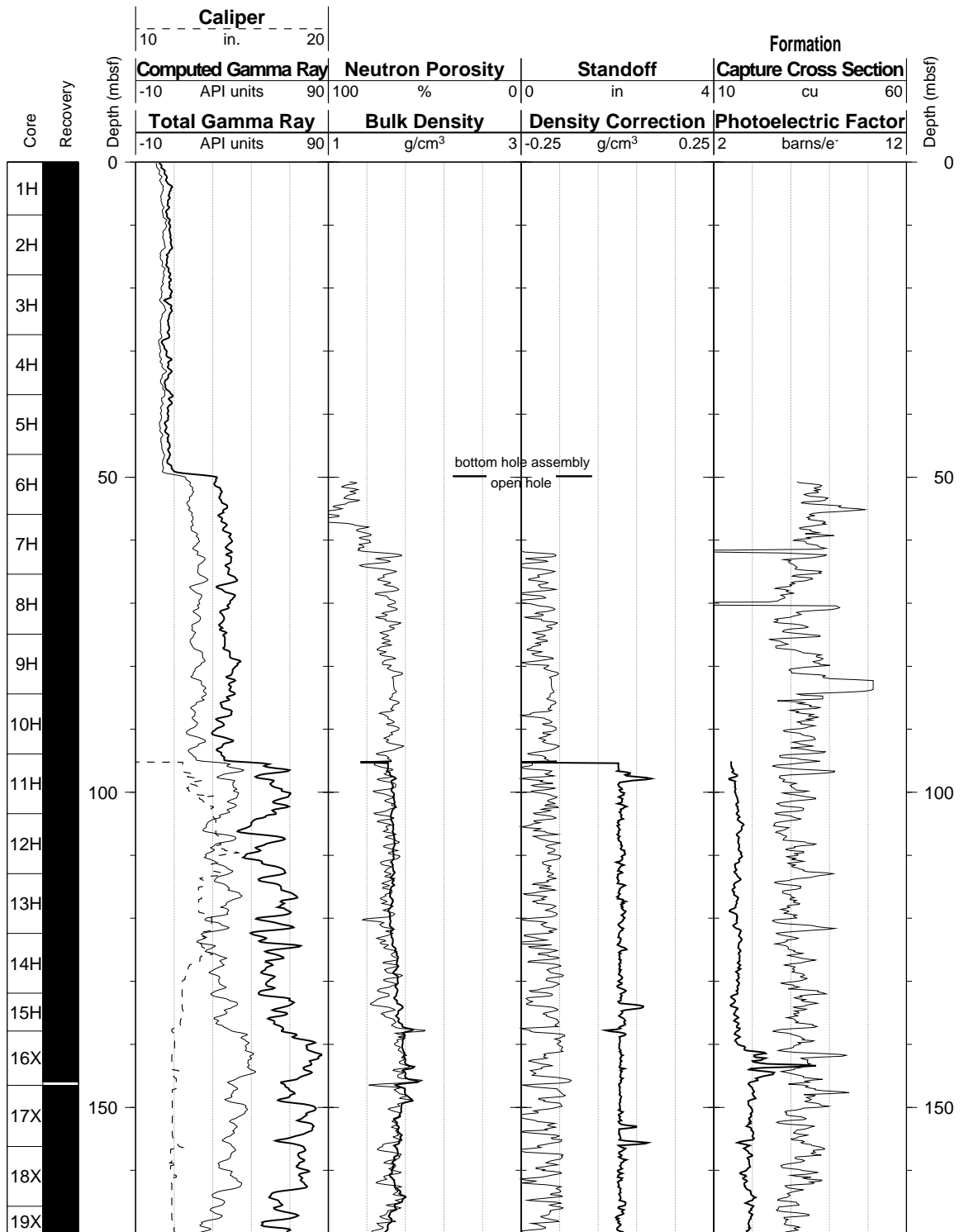
Hole diameter was recorded by the hydraulic caliper on the HLDT tool (CALI) and the caliper on the FMS string (C1 and C2).

Note: Details of standard shore-based processing procedures are found in the "Explanatory Notes" chapter, this volume. For further information about the logs, please contact:

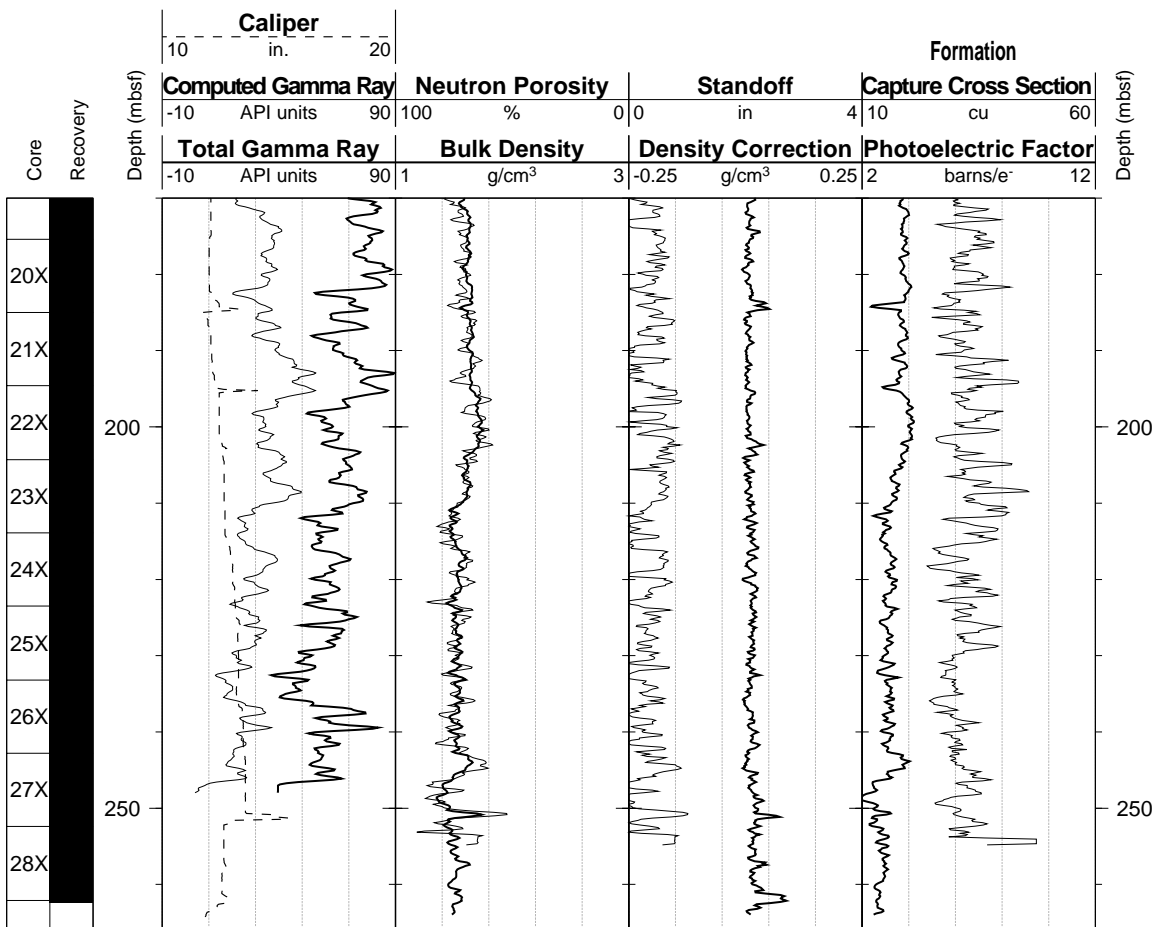
Cristina Broglia
Phone: 914-365-8343
Fax: 914-365-3182
E-mail: chris@ldeo.columbia.edu

Zhiping Tu
Phone: 914-365-8336
Fax: 914-365-3182
E-mail: ztu@ldeo.columbia.edu

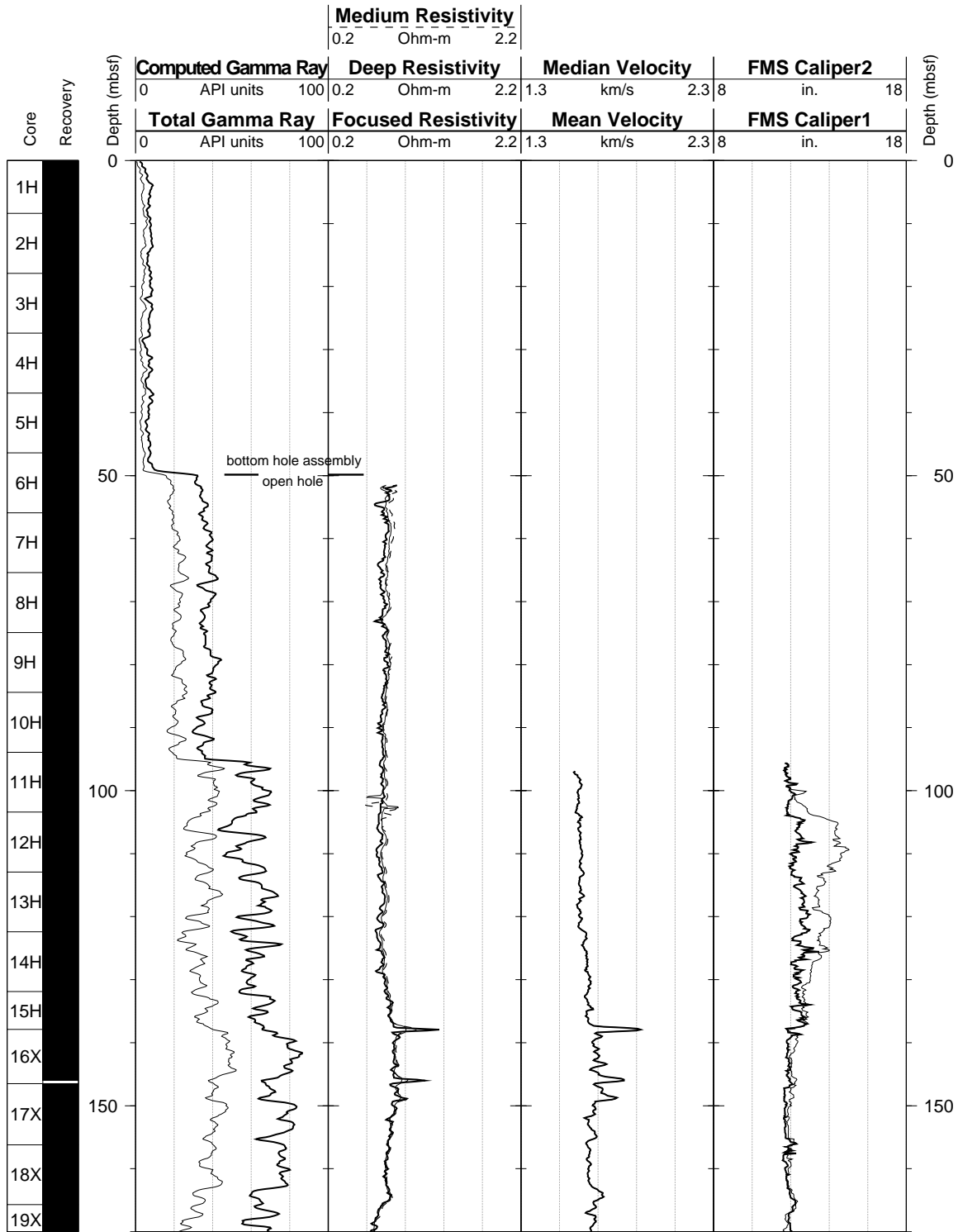
Hole 1011B: Natural Gamma Ray-Density-Porosity Logging Data-Pass 2



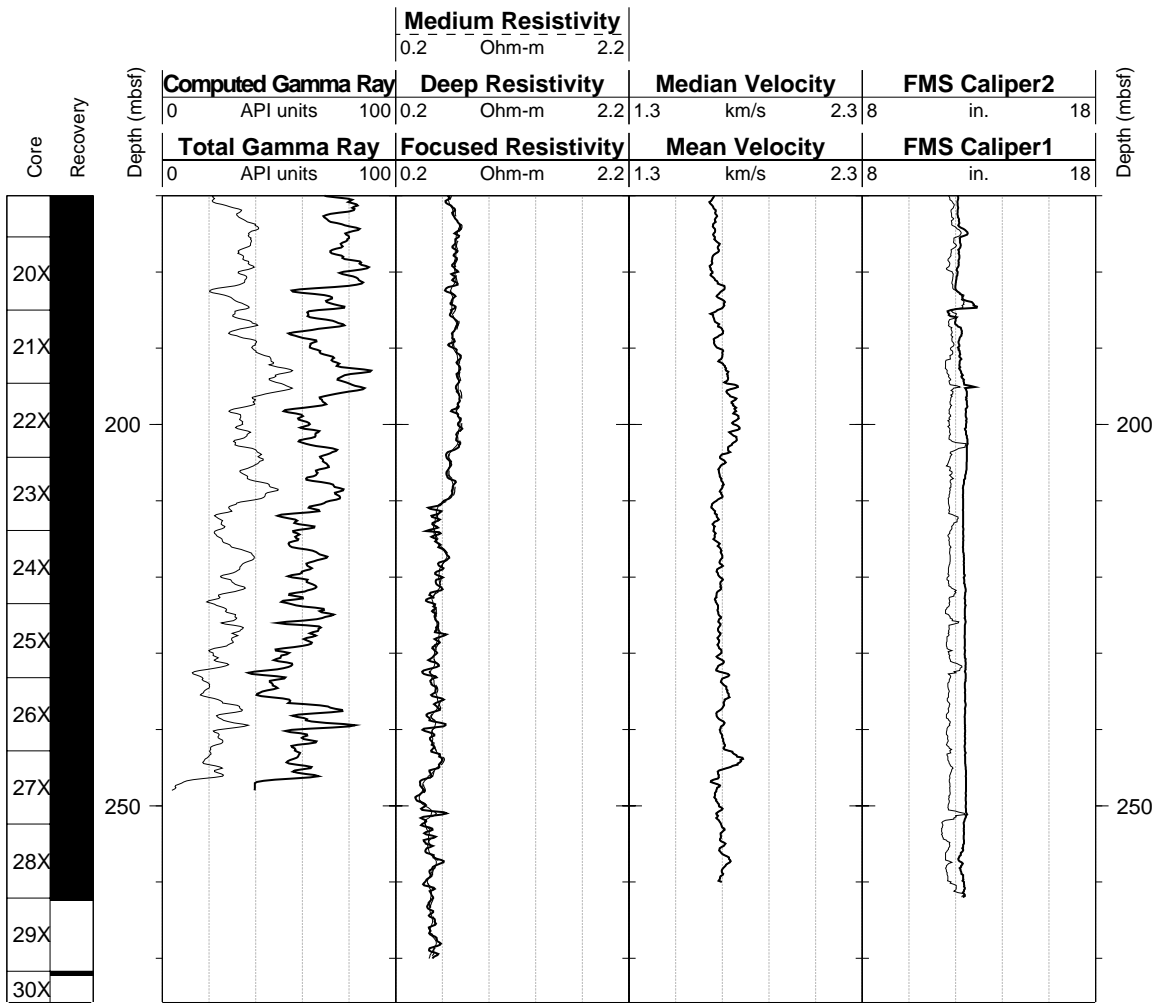
Hole 1011B: Natural Gamma Ray-Density-Porosity Logging Data-Pass 2 (cont.)



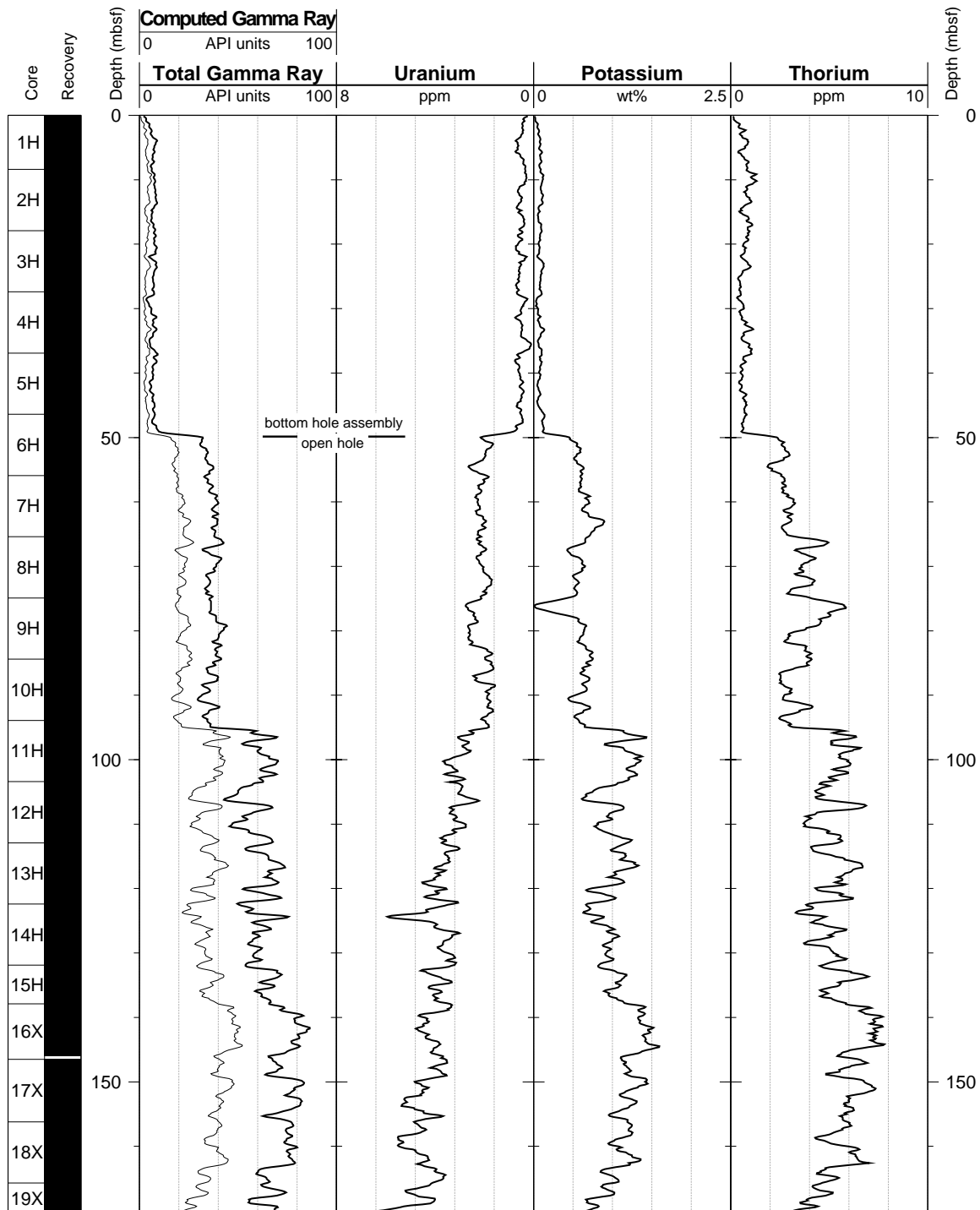
Hole 1011B: Natural Gamma Ray-Resistivity-Sonic Logging Data-Pass 2



Hole 1011B: Natural Gamma Ray-Resistivity-Sonic Logging Data-Pass 2 (cont.)



Hole 1011B: Natural Gamma Ray Logging Data-Pass 2



Hole 1011B: Natural Gamma Ray Logging Data-Pass 2 (cont.)

